1 **Investigation of an extreme rainfall event during 8–12 December 2018 over central**

2 **Viet Nam – Part 2: An evaluation of predictability using a time-lagged cloud-resolving**

3 **ensemble system**

4 Chung-Chieh Wang[1], Duc Van Nguyen[1,2], Thang Van Vu[2], Pham Thi Thanh Nga[2], Pi-Yu

5 Chuang[1], and Kien Ba Truong[2,*]

6 Correspondence: kien.cbg@gmail.com

7 [1]Department of Earth Sciences, National Taiwan Normal University, Taipei, Taiwan

8 [2]Viet Nam Institute of Meteorology, Hydrology and Climate Change, Hanoi, Viet Nam

9 **Abstract:**

10 This is the second part of a two-part study that investigates an extreme rainfall event that

11 occurred from 8 to 12 December 2018 over central Viet Nam (referred to as the D18 event).

12 In this part, the study aims to evaluate the predictability of the D18 event using a time-

13 lagged cloud-resolving ensemble and a quantitative precipitation forecast system. To do

14 this study, 29 time-lagged (8 days in lead time) high resolution (2.5 km) members were

15 run, with the first members run at 12:00 UTC 3 December 2018, and the last member-run

16 at 12:00 UTC 10 December 2018. Between the first and the last members are multiple

17 members that run every 6-h. The evaluated results reveal that the could-resolving model

18 (CReSS) well predict the rainfall fields at the short-range forecast (less than 3 days) for 10

19 December (rainiest day). Particularly, results show CReSS has high skills in heavy-rainfall

20 quantitative precipitation forecasts (QPFs) for the 24-h rainfall of 10 Dec with the

21 Similarity Skill Score (SSS) scores greater than 0.5 for both the last five members and the

22 last nine members. These good results are due to the model having good predictionsof other

23 meteorological variables, such as surface wind fields. However, these prediction skills are

24 reducing at extending lead time (longer than 3 days), and it is challenging to achieve the

25 prediction of QPF for rainfall thresholds greater than 100 mm with lead time longer than 6

26 days. Besides, the ensemble sensitivity analysis of 24-hour rainfall responds to the initial

27 conditions shows that the 24-hour rainfall is very sensitive with initial conditions, not only

at the lower level but also at the upper level. The ensemble-based sensitivity is decreased with the increasing lead time. Through the analysis of thermodynamic and moisture sensitivities, it showed that the features of the ensemble-based sensitivity analysis (ESA) facilitated a better understanding of the sensitivity of a precipitation forecast to the initial conditions, implying that it is meaningful to apply ESA to control initial conditions by work in the future.

1 Introduction

The present study is the second part of a two-part study investigating the extreme rainfall event during 8–12 December 2018 over central Viet Nam (referred to as the D18 event hereafter). D18 event is a record-breaking rainfall event which occurred along the mid-central coast, from Quang Binh to Quang Ngai provinces. The observational data shows that particularly heavy rainfall with the maximum 3-days accumulated rainfall from 12:00 UTC on 8 December to 12:00 UTC on 11 December exceeding 800 mm (Fig. 1f). In which, the rainiest day is 10 December with 24-h observed data exceed 600 mm at some stations (Fig. 4 OBS). This record-breaking rainfall event led to 13 dead, many destructions in the environment, downstream cities, and many other economic losses due to catastrophic flooding and landslides (Tuoi Tre news, 2018). In part 1 (Wang and Nguyen 2023), we focused on the analysis of the mechanism that caused this event and evaluated the simulation by the Cloud-Resolving Storm Simulator (CReSS; Tsuboki and Sakakibara, 2002, 2007). The analyzed results point out the main factors which led to this event as well as its spatial rainfall distribution. These factors included the combined interaction between the strong northeasterly winds and easterly winds over the South China Sea (SCS) in the lower troposphere (below 700 hPa). The local terrain also played essential role due to its barrier effect. The cloud model's good simulation results in part 1 indicated its promising potential in forecasting this event. Hence, in part 2, the present study focuses on an evaluation of its predictability of the D18 event through a series of time-lagged high resolution ensemble quantitative precipitation forecasts by the CReSS model.

Until now, predicting heavy rainfall events is still challenging to meteorologists and weather forecasters, although great progresses in both computer science and atmospheric science have been made to improve predictability. The prediction of heavy to extreme rainfall is more difficult for Viet Nam, where both multi-scale interactions among different weather systems and strong influence by local topography often exist. For example, when D18 event occurred, several operational models were unable to predict this event successfully. Specifically, Fig. 1 shows the predictions for the D18 event by three global models at the National Centers for Environmental Prediction (NCEP), the European Centre for Medium-Range Weather Forecasts (ECMWF), and the Japan Meteorological Agency (JMA), and by one mesoscale regional model, the Weather Research and Forecasting (WRF) model, implemented for operation at the Mid-central regional Hydro-Meteorological center in Da Nang city, Viet Nam. While these models overall made good predictions in the surface wind field, their 72-h accumulated rainfall amounts along the coast of central Viet Nam (less than 250 mm) were much lower than the observation, which exceeded 900 mm (Fig. 1). Therefore, in order to improve the QPFs for heavy rainfall events in Viet Nam, we need to not only understand their mechanisms of occurrence, but also develop better forecasting tools.

77
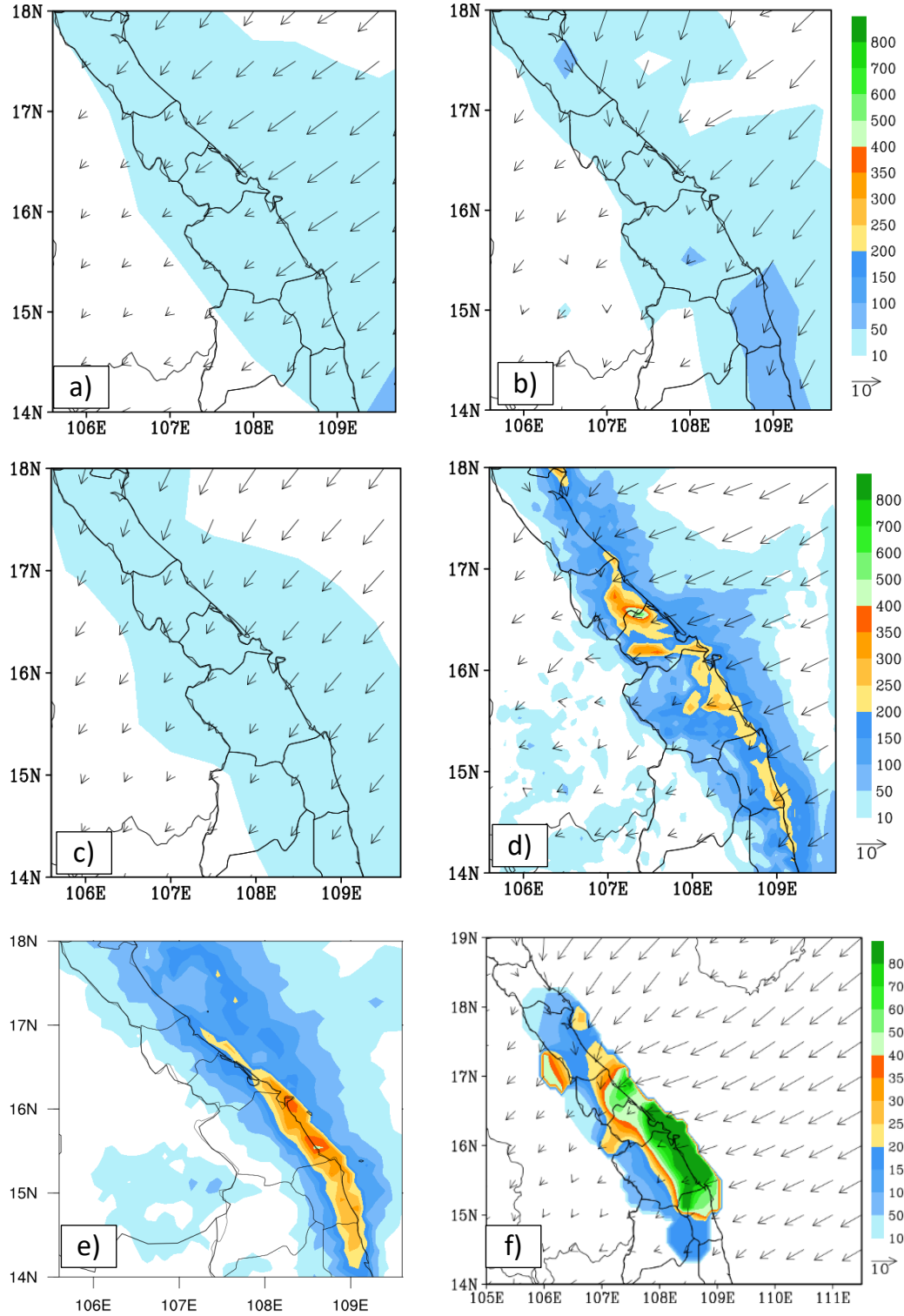
Figure 1. The predicted 72h accumulated rainfall (mm, shaded) and mean surface wind
(ms^{-1}, vector) for the period of 12:00 UTC 8 December – 12:00 UTC 11 December 2018

obtained by (a) NCEP, (b) ECMWF, (c) JMA, (d) WRF, (e) 72h accumulated rainfall obtained by the Global Precipitation Measurement (GPM) estimate (IMERG Final Run product) and (f) 72h in-situ observed accumulated rainfall (mm, shaded) and the mean surface wind derived from ERA5 data (ms^{-1}, vector), adapted from Fig. 14c of Wang and Nguyen 2023.

Among several different methods, the present-day weather forecasts depend mainly on numerical weather prediction (NWP) using models, a scientific method that has become indispensable for its ability to simulate weather and produce quantitative results (Fig. 1). However, there is always uncertainty in the numerical forecasts due to the fact that the atmosphere is a chaotic system and tiny errors in the initial state can grow rapidly and lead to large errors in the forecast (Hohenegger and Schär, 2007, Lorenz 1969). Various approximations in numerical methods are also sources of forecast uncertainty. Thus, by generating a range of possible weather conditions in days ahead or into the future, the ensemble forecasting was introduced as an effective method to estimate forecast uncertainty and improve the overall accuracy and usefulness of NWP products. For example, some studies have shown high skill in QPFs for extreme rainfall produced by typhoons in Taiwan using the CReSS model, a cloud-resolving model (CRM), with high resolution and time-lagged approach (Wang et al. 2016; Wang 2015; Wang et al. 2014; Wang et al. 2013). Table 1 of Wang et al. (2016) shows that the high-resolution time-lagged ensemble forecasts provide overall better quality in comparison with both the traditional low-resolution ensemble forecasts and high-resolution deterministic forecasts at a comparable cost in computation. Furthermore, some studies show that the ensemble mean typically has smaller errors than individual members (Murphy 1988, Surcel et al. 2014). This error reduction is because the high predictability features that the members agree on are emphasized by the mean, while the low-predictability ones that the members do not agree on are filtered out or dampened (e.g., Leith 1974; Murphy 1988, Surcel et al. 2014).

Besides the advantages of ensemble forecasts described above, the ensemble-based sensitivity analysis also helps effectively investigate how sensitive the forecast variables

108   are and to what preceding factors. To be more specific, Torn and Hakim (2009) used ESA

109   to evaluate how their subject, tropical cyclones (TCs) undergoing extratropical transition,

110   in the prediction respond to a change in the initial condition. In their results, the cyclone

111   minimum sea-level pressure forecasts are determined as strongly sensitive to TC intensity

112   and position at short lead times and equally sensitive to mid-latitude troughs that interacted

113   with the TC at longer lead times. For an extreme rainfall event in northern Taiwan, Wang

114   et al. (2021) performed ESA using the results from 45 forecast members with a grid size

115   of 2.5–5 km to identify contributing factors to heavy rainfall. By normalizing their impacts

116   on rainfall using standard deviation (SD), different factors can be compared quantitatively

117   and on an equal footing. Ranked by their importance, these factors included the position of

118   the surface Mei-yu front and its moving speed, the position of 700-hPa wind shift line and

119   its speed, the moisture amount in the environment near the front, timing and location of

120   frontal mesoscale low-pressure disturbance, and frontal intensity. Many other studies also

121   used the ESA to study TCs, convective events, or support the development of operational

122   ensemble sensitivity-based techniques to improve probabilistic forecasts (Kerr et al. 2019,

123   Hu and Wu 2020, Coleman and Ancell 2020).

124   For heavy precipitation over central Viet Nam, Son and Tan (2009) used the Mesoscale

125   Model version 5 (MM5) to investigate the predictability of heavy rainfall events over the

126   southern part of central Viet Nam during the period of 2005 and 2007. In this

127   study,experiments were configured for two domains with the horizontal resolutions of the

128   mother domain and the nest domain are 27km and 9km, respectively. Their results showed

129   that MM5 can predict heavy rainfall there and its performance is better for events caused

130   by TCs or TC interactions with the cold air. Toan et al. (2018) assessed the predictability

131   of heavy rainfall events in middle-central Viet Nam due to combined effects of cold air and

132   easterly winds using the WRF model within a forecast range of 2 days. The model was set

133   with two domains using the nesting technique. The outermost domain (D1) covers entirely

134   Vietnam and South China Sea with horizonal resolution of 18 km, while the inner domain

135   (D2) focuses on the Mid-Central Vietnam region with horizonal resolutions of 6km. The

136 evaluation indicated that for 24-h lead time, the model performed reasonably well at

137 rainfall thresholds less than 100 mm day^{-1}. For 48-h forecast range, the model performed

138 well only at thresholds below 50 mm day^{-1} and had some skill at 50–100 mm day^{-1}.

139 However, heavy rainfall events at thresholds over 100 mm day^{-1} were almost unpredictable

140 by the model. Nhu et al. (2017) also used the WRF model to investigate the role of the

141 topography in central Viet Nam on the occurrence of a heavy rainfall event there in

142 November 1999. In this study, the model with 3 nested domains with horizontal resolution

143 of 45km, 15km, 5km and 47 vertical levels well simulated the northeast monsoon

144 circulation, TCs, and the occurrence of heavy rainfall in central Viet Nam. Furthermore,

145 when the topography is removed, the three-day total accumulated rainfall decreased

146 sharply (by approximately 75%) compared to that in the control experiment with the

147 terrain. Hoa Van Vo (2016) examined the predictability of heavy-rainfall events during the

148 wet seasons of 2008−2012 in the middle section and central highlands of Viet Nam using

149 NWP products from several global models, including the Global Forecasting System (GFS)

150 from NCEP, Global Spectral Model (GSM) from JMA, Navy Operational Global

151 Atmospheric Processing System (NOGAPS) from the US Navy, and the Integrated

152 Forecast System (IFS) from ECMWF. Their results indicated that IFS and GSM performed

153 better than GFS and NOGAPS, and IFS was evaluated the best. However, all four global

154 models under-estimated rainfall in extreme events. One of the reasons for this under-

155 estimated rainfall is that these models are global models, so their resolutions are coarse

156 while the study area is too small. The review above suggests that considerable limitations

157 still exist in forecasting heavy rainfall in central Viet Nam, especially using coarser models.

158 It also indicates that a high-resolution time-lagged ensemble approach may offer some

159 advantages in the prediction of extreme rainfall events, such as a better simulation of local

160 weather conditions, a quicker response to changes in forecast uncertainty in real time, and

161 potentially a longer lead time for hazard preparation. Climatologically, the entire Viet Nam

162 lies in the tropical zone (Fig. 2a), where vigorous but less organized convection often

163 develops in response to local conditions, while the region is also prone to the influence and

164 interactions of weather systems spanning a wide range of scales as reviewed. In addition,

165 although central Viet Nam is a small region with the narrowest place only about 80 km in

166 width, it possesses significant topography running in the north-south direction to affect

167 rainfall (Fig. 2a). Hence, a high-resolution CRM with detailed and explicit treatment in

168 cloud microphysics is likely crucial for better QPFs in central Viet Nam. Consequently,

169 the present study used the CReSS model to investigate the predictability of the D18 event

170 through a series of time-lagged ensemble predictions. The rest of this paper is organized as

171 follows. Section 2 describes the data, model, and methodology used in the study. The

172 model results are presented and evaluated in Section 3. Finally, conclusions are offered in

173 Section 4.

174 **2 Data and methodology**

175 2.1 Data

176 2.1.1 Model validation

177 *2.1.1.1 In-situ observation data*

178 The daily in-situ observed rainfall data (12:00–12:00 UTC, i.e., 19:00–19:00 LST) from 8

179 to 12 December 2018 at 69 automated gauge stations across central Viet Nam is used for

180 case overview and verification of model results. This dataset is provided by the Mid-

181 Central Regional Hydro Meteorological Center, Viet Nam. The spatial distribution of these

182 gauge stations is depicted in figure 2b.

183 *2.1.1.2 The Global Precipitation Measurement (IMERG Final Run V07) data*

184 The Global Precipitation Measurement (GPM) is a mission international jointly by the

185 National Aeronautics and Space Administration (NASA) and the Japan Aerospace

186 Exploration Agency (JAXA), employing an international satellite network for advanced

187 global rain and snow observations. The GPM *IMERG Final Run* is a research-level product

188 which is created by intercalibrate, merging, and interpolating "all" satellite microwave

189 precipitation estimates, along with microwave-calibrated infrared (IR) satellite estimates,

analyses from precipitation gauges, and potentially other precipitation estimation methodologies at fine time and space scales. The horizontal resolution of this dataset is 0.1⁰ ×0.1⁰ latitude–longitude and the time resolution is every 30 minute (). In this study, we used this satellite data (version 7) to verify rainfall distribution over the coastal sea due to the limitation of the observation station network, we only have the observation stations inland, as shown in the Fig. 2b. This dataset was downloaded from 12:00 UTC on 8 December to 12:00 UTC on 11 December 2018 to analyze the D18 event as well as the rainiest day of this event (10 December).2.1.1.3 NCEP GDAS/FNL global tropospheric analyses data

The present study used this data (version d083003) to verify the initial data and the model output. The NCEP FNL analysis data is an operational global gridded analysis data and is freely provided by NCEP. The horizontal resolution of this dataset is $0.25^{o} \times 0.25^{o}$ latitude–longitude with 26 levels extending from the surface to 10 hPa. The temporal resolution is 6 hours. Variables have been used in this study including the zonal and meridional wind components, relative humidity and vertical velocity at 925 hPa, and downloaded from 18:00 UTC 04 to 12:00 UTC 09 December 2018.

2.1.2 The added values of CReSS ensemble

2.1.2.1 The International Grand Global Ensemble retrieval

In this study, we used the global model predictions to analyze the predictability of the D18 event. The International Grand Global Ensemble (TIGGE) retrieval is a key component of The Observing System Research and Predictability Experiment (THORPEX) research program, whose aim is to accelerate the improvements in the accuracy of 1-day to 2-week high-impact weather forecasts. The TIGGE retrieval provides not only deterministic forecast data but also ensemble prediction datasets from major centers, including NCEP of the USA, , ECMWF of the European countries, and JMA of Japan, since 2006. This dataset has been used for a wide range of research studies on predictability and dynamical processes. the variables utilized included total precipitation and surface winds (*u*- and *v*-

217 wind components at 10-m height) from NCEP, ECMWF, and JMA at 6-h intervals during
218 our data period (as shown in Figs. 1a-c) from 12:00 UTC 8 to 12:00 UTC 11 December
219 2018 (as shown in Figs. 1a-c). The data linked is placed in the "code and data availability"
220 section.

221 *2.2 The WRF data*

222 The WRF is implemented for operational numerical forecast system at Mid-central regional
223 Hydro- Meteorological center, Viet Nam. In this study, we used this data to analysis the
224 predictability of D18 event using the mesoscale numerical prediction. The download
225 variables include precipitation, the surface U wind component and surface V wind
226 component. The lead time is 3 days, starting from 12:00 UTC 8 to 12:00 UTC 11 December
227 2018 with interval time of 6 hours. The horizontal resolution of this data is 6 km x 6 km.

228 2.2.1 Model description and experiment setup

229 We used the could-resolving model (CReSS). This model had been built and developed by
230 Nagoya University, Japan (Tsuboki and Sakakibara, 2002, 2007). This is a non-hydrostatic
231 and compressible cloud model, designed for simulation of various weather events at high
232 (cloud-resolving) resolution. In the model, the cloud microphysics is treated explicitly at
233 the user-selected degree of complexity, such as the bulk cold-rain scheme with six species:
234 vapor, cloud water, cloud ice, rain, snow, and graupel (Lin et al., 1983; Cotton et al., 1986;
235 Murakami, 1990, 1994; Ikawa and Saito, 1991). Other subgrid-scale processes
236 parameterized, such as turbulent mixing in the planetary boundary layer, as well as physical
237 options for surface processes, including momentum/energy fluxes, shortwave and
238 longwave radiation are summarized in Table 1.

239 Besides, the NCEP GFS data (version ds084.6) from the analyses and deterministic
240 forecast runs executed every 6 h, at 00:00, 06:00, 12:00, and 18:00 UTC daily, were used
241 to drive the CReSS model predictions. The horizontal resolution of the data is 0.25° ×
242 0.25°, and 26 of vertical levels, and the forecast fields are provided every 3 h from the

243 initial time out to a range of 192 h. The data linked is also placed in the "code and data
244 availability" section.

245 To evaluate of the predictability of the D18 event using an ensemble time-lagged high-
246 resolution system and investigate the ensemble sensitivity of variables for the rainfall, 29
247 experiments were performed. The first member was initialized at 12:00 UTC on 3
248 December 2018, and the last member was initialised at 12:00 UTC on 10 December 2018.
249 A new member was initialised every 6-hr within the period 1200 UTC 3 Dec 2018-1200
250 UTC 10 Dec 2018 (for a simulation length of 192 h).

251 All experiments using a single domain at 2.5 km horizontal grid spacing and a (x, y, z)
252 dimension of 912 x 900 x 60 grid points (Table 1, cf. Figure 2). As introduced above, the
253 NCEP GFS was used as the IC/BCs of the model.

254
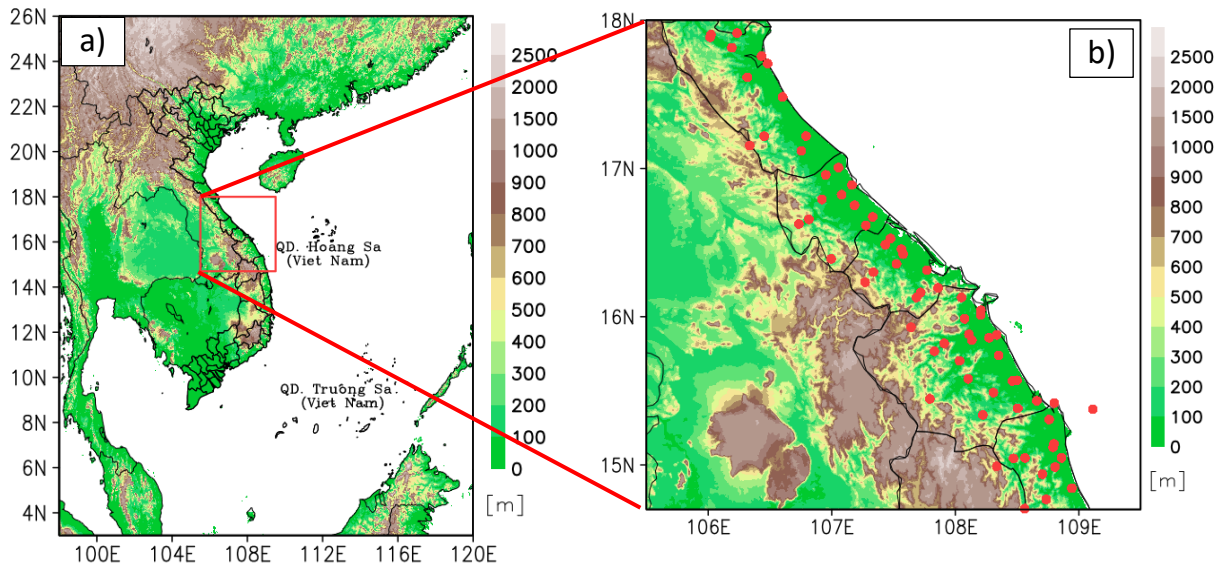
255 **Figure 2**. (a) The simulation domain of the CReSS model and topography (m, shaded)
256 used in the study. The red box marks the study area. (b) The distribution of the
257 observation stations (red dots) in the study area.

258

259

260   Table 1. The basic information of experiments.

Domain and Basic setup	
Model domain	3°–26°N; 98°–120°E
Grid dimension (x, y, z)	912 × 900 × 60
Grid spacing (x, y, z)	2.5 km × 2.5 km × 0.5 km*
Projection	Mercator
IC/BCs (including SST)	NCEP GDAS/FNL Global Gridded Analyses and Forecasts (0.25° × 0.25°, every 6 h, 26 pressure levels)
Topography (for CTRL only)	Digital elevation model by JMA at (1/120)° spatial resolution
Simulation length	192 h
Output frequency	1 hour
Model physical setup	
Cloud microphysics	Bulk cold-rain scheme (six species)
PBL parameterization	1.5-order closure with prediction of turbulent kinetic energy (Deardorff, 1980; Tsuboki and Sakakibara, 2007)
Surface processes	Energy and momentum fluxes, shortwave and longwave radiation (Kondo, 1976; Louis et al., 1982; Segami et al., 1989)
Soil model	41 levels, every 5 cm deep to 2 m

261   * The vertical grid spacing (Δz) of CReSS is stretched (smallest at bottom) and the

262   averaged value is given in the parentheses

263   2.3 Verification of model rainfall

264   In order to verify the model-simulated rainfall, some verification methods are used,

265   including (1) visual comparison between the model and the observation (from the 69

266   automated gauges over the study area), and (2) the objective verification using categorical

267   skill scores at various rainfall thresholds from the lowest at 0.05 mm up to 900 mm for

268   three-day total. These scores are presented below along with their formulas, perfect value,

269   and worst value, respectively. To apply these scores at a given threshold, the model and

270   observed value pairs at all verification points (gauge sites here, N) are first compared and

271   classified to construct a 2×2 contingency table (Wilks, 2006). At any given site, if the

272   event takes place (reaching the threshold) in both model and observation, the prediction is

273   considered a hit (*H*). If the event occurs only in observation but not the model, it is a miss

274   (*M*). If the event is predicted in the model but not observed, it is a false alarm (*FA*). Finally,

275   if both model and observation show no event, the outcome is correct rejection (*CR*). After

276   all the points are classified into the above four categories, the scores can be calculated by

277   their corresponding formula as:

278   Bias Score (BS) = (H+FA)/(H+M),   (1)

279   Probability of Detection (POD) = H/(H+M),   (2)

280   False Alarms Ratio (FAR) = FA/(H+FA),   (3)

281   Threat Score (TS) = H/(H+M+FA),   (4)

282   The values of TS, POD, and FAR are all ranged from 0 to 1, and the higher value is the

283   better for TS and POD, and conversely for FAR. For BS, its value can vary from 0 to N−1

284   and indicate the overestimation (underestimation) of the model for the events.

285   2.3.1 The Similarity Skill Score

286 In addition to the categorical scores, the Similarity Skill Score (SSS, Wang et al., 2022) is

287 also applied to evaluate the model rainfall results, as

288
$$\text{SSS} = 1 - \frac{\frac{1}{N}\sum_{i=1}^{N}(F_i - O_i)^2}{\frac{1}{N}\sum_{i=1}^{N}F_i^2 + \frac{1}{N}\sum_{i=1}^{N}O_i^2} \qquad (5)$$
289

290 where N is the total number of verification points, F_i is the forecast rainfall amount, and O_i

291 is the observed value, at the ith point among N, respectively. The SSS is a measure against

292 the worst mean squared error (MSE) possible. The formula shows that a forecast with

293 perfect skill has an SSS of 1, while a score of 0 means zero skill (model rainfall does not

294 overlap with the observation anywhere).

295 2.3.2. The ensemble spread (standard deviation)

296 The ensemble spread is considered a measure of the difference between the members to

297 the ensemble mean and known as the standard deviation (SD). In other words, the ensemble

298 spread will reflect the diversity of all possible outcomes. Hence, the ensemble spread is

299 often applied to predict the magnitude of the forecast error. For example, small spread

300 indicates high theoretical forecast accuracy, and large spread indicates low theoretical

301 forecast accuracy. Spread is computed by formulated below:

302
$$\text{SD} = \sqrt{\frac{\sum_{i=1}^{n}(x_i - \mu_x)^2}{n-1}}$$
303 $\qquad (6)$

304 where x_i is the prediction value of member i, μ_x is the ensemble mean, n is the number of

305 ensemble members.

306 2.3.3. Ensemble Sensitivity Analysis

307 As mentioned above, an ensemble forecast is a set of forecasts produced by many separate

308 forecasts with differences in initial conditions, respectively. Moreover, as we know, the

309 numerical weather forecasts are sensitive to small changes in initial conditions and

310 sensitivity analysis is considered a measure to improve forecasts through targeting

311   observations. Hence, this study used the ESA method which is introduced by Ancell and

312   Hakim (2007) to examine how a forecast variable responds to changes in initial conditions.

313   The ensemble sensitivity is computed by the formula:

314
$$\frac{\partial R}{\partial x_t} = \frac{COV(R,x_t)}{var(x_t)} \qquad (7)$$

315   Here, the response function R is chosen to be the areal-mean 24-h accumulated rainfall in

316   central Viet Nam (15.5°-16.3°N, 107.9°-108.6°E) on the rainiest day, from 12:00 UTC on

317   9 to 12:00 UTC on 10 December 2018. The starting time of this period, i.e., 12:00 UTC on

318   9 December, is defined as t_0. Various scalar variables are considered for x_t, while those

319   from 48 h earlier (t_{-48}, or 12:00 UTC on 7 December) to the time of t_0 at 24-h intervals.

320   The COV is the covariance of R and x_t, and var is the variance of x_t, respectively.

321   As the analysis in part 1, the D18 event is caused by combined effectively between the

322   atmospheric disturbances at lower levels, such as cold surge, easterly wind, and

323   topography, ensemble-based sensitivity analysis (ESA) has been applied for variables at

324   surface, near-surface, and mid-tropospheric levels to assess the sensitivity of initial

325   conditions to the predictability of the rainy field. In order to facilitate the comparison

326   among the impacts of different variables, this study normalized ESA results by using the

327   standardized anomaly in the denominator and expressed as the change in R (in mm) in

328   response to an increase in x_t by one SD.

329   **3 Model results**

330   3.1 Time-lagged 24-h QPFs by the CReSS model

331   In this section, time-lagged forecasts targeted for the 24-h period from 12:00 UTC on 9 to

332   12:00 UTC on 10 December in the D18 event by the 2.5-km CReSS model are presented

333   and evaluated. This study focuses on this 24-h period because this is the rainiest day with

334   24-h in-situ observed data exceeding 600 mm at some stations (Fig. 3 OBS). Figure 3

335   shows 25 possible scenarios of 24-h rainfall and average surface winds over the target

336   period produced by the lagged runs every 6 h, with the earliest initial time at 12:00 UTC

337   on 3 December and the latest one at 12:00 UTC on 9 December 2018, respectively. It is

338   immediately clear that several members made a rather good 24-h QPF not only in amounts,

339   but also in rainfall location and spatial distribution. These include most members initialised

340   during 8-9 December, and also an impressive member that initialised at 18:00 UTC on 4

341   December. In this latter member, a reasonably good QPF was produced at a rather long

342   lead time, almost five days prior to the beginning of the target period (114 h). A common

343   feature among these good members is that they all captured the direction and magnitude of

344   surface winds quite well. On the other hand, most other members did poorly in their QPFs,

345   when initialised before 06:00 UTC on 7 December at lead times beyond two days before

346   the target period. In general, they also could not predict the surface winds well enough.

347

00:00 UTC 9   06:00 UTC 9   12:00 UTC 9
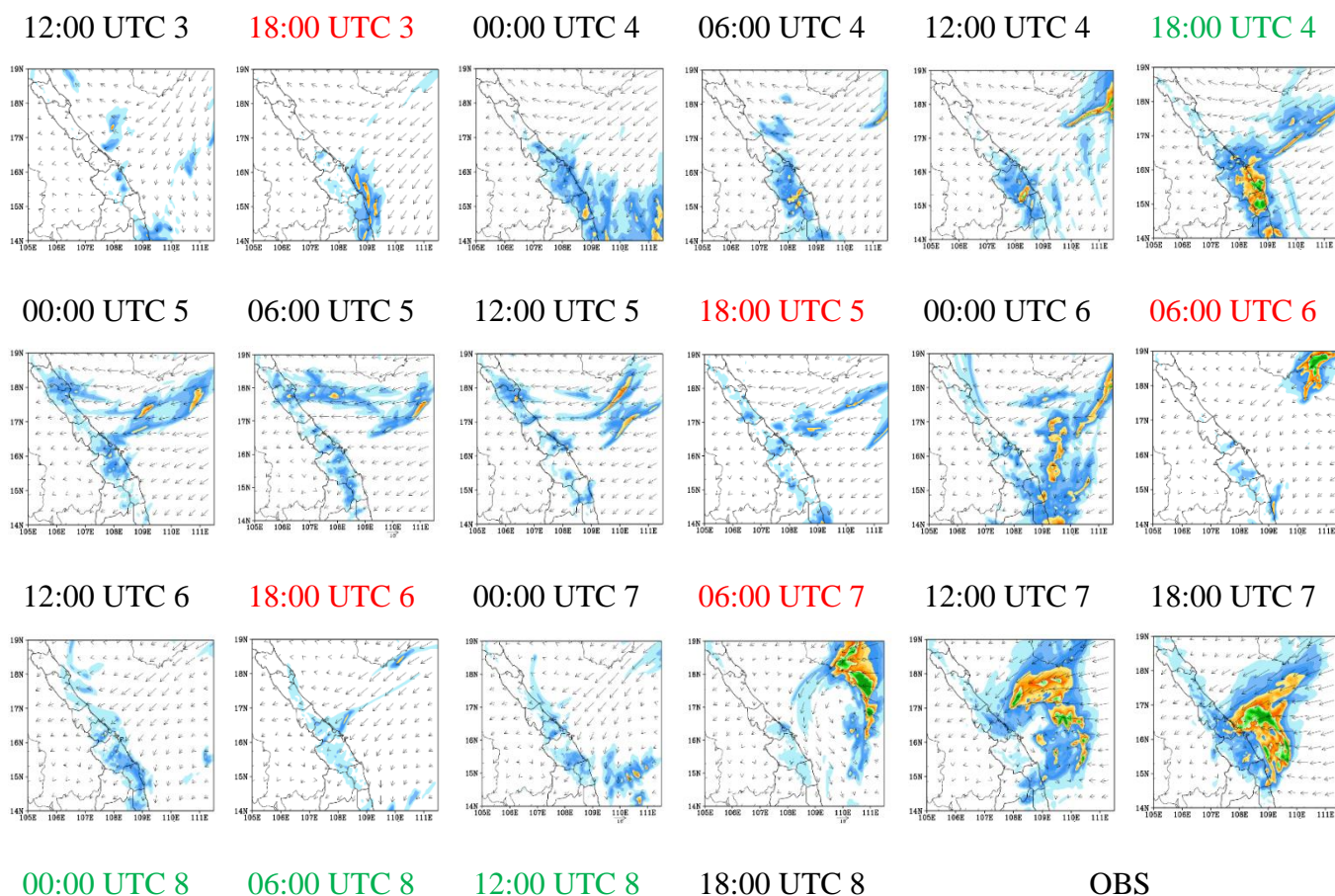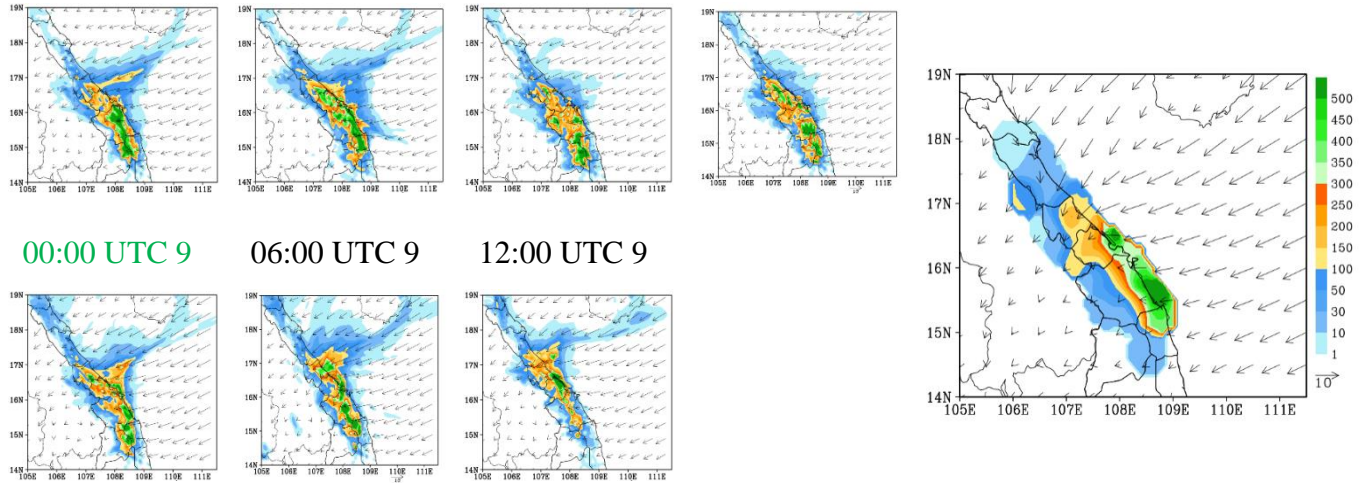
Figure 3. The predicted 24h accumulated rainfall (mm, shaded, scale on the right of panel OBS) and the mean surface horizontal wind (ms^{-1}, vector, reference length at panel OBS) on 10 December 2018 (from 12:00 UTC 9 December to 12:00 UTC 10 December 2018). The green color mark good members and the red color marks bad members. In OBS, 24h in-situ observed rainfall (mm, shaded) and the surface wind derived from ERA5 data (ms^{-1}, vector), adapted from Fig. 12f of Wang and Nguyen 2023.Furthermore, as we know, ensemble weather forecasts are a set of forecasts from multiple members that represent the range of future weather possibilities, and the simplest way to use them is through the ensemble mean (that emphasizes the features that the members agree upon). In order to see how good CReSS can predict the D18 event with the time-lagged strategy, from possible scenarios of 24 hours of rainfall of 10th December that produced by CReSS, This study has grouped scenarios and computed them into different lead times using the range of their initial times. It can be clearly seen in Fig. 4 that the rainfall produced by Fifth 4 (12 UTC 7 - 06 UTC 8 Dec) and Sixth 4 (12 UTC 8 - 06 UTC 9 Dec) members is quite similar to observed data, not only rainfall amount but also the locations of significant rainbands and regions that concentrate mainly rainfall. For other subgroup scenarios, the model made the rainfall scenarios much lower than observed rainfall data. In which, third 4 (12 UTC 5 - 06 UTC 6 Dec) and fourth 4 (12 UTC 6 - 06 UTC 7 Dec) members are the lowest. It can be relevant to the model that did not predict well the wind fields in every single running at extend ranges (after day 3) as analyzed previous. The rainfall of second 4 (12 UTC 4 - 06

UTC 5 Dec) members is the highest in these subgroup scenarios due to a single good forecast initialised at 1800 UTC on 4 Dec [Fig. 3. (18:00 UTC 4)].
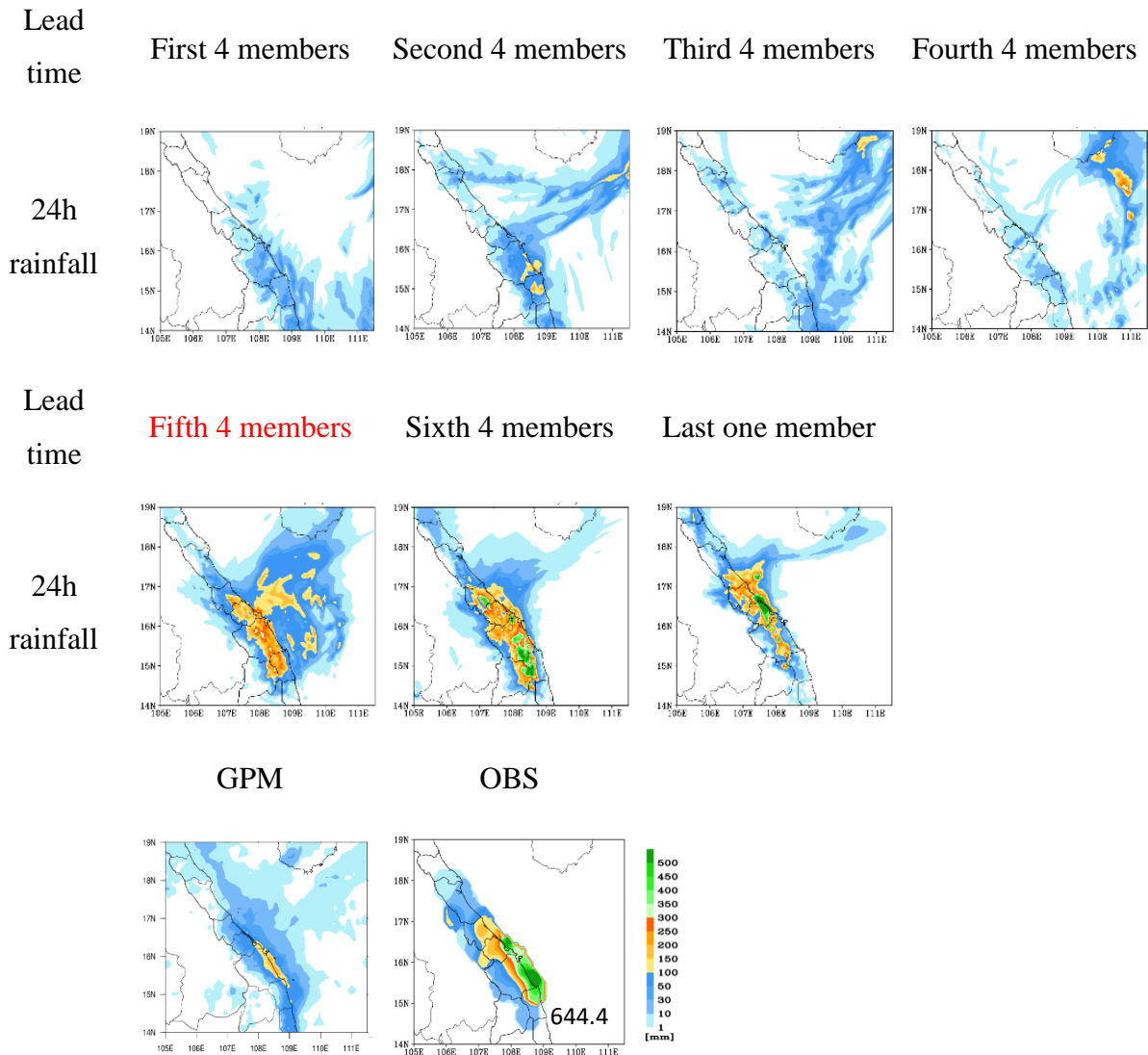
Figure 4. The predicted 24h rainfall by subgroup members, 24h accumulated rainfall by the Global Precipitation Measurement (GPM) estimate (IMERG Final Run product), 24h observed rainfall (mm, peak amount labeled at the lower-right corner) for the period of 12:00 UTC 9 December – 12:00 UTC 10 December 2018 as labelled. The same color bar (lower right) is used for all panels.

376   Besides the evaluation on time-lagged results using batches of fixed number of successive
377   runs (every 4 members) as presented above, this study also grouped the members using
378   different ensemble sizes based on their behavior in order to better assess the temporal
379   evolution of forecast uncertainty and event predictability as the lead time shortened.
380   Particularly, this study divided the 25 members into several subgroups as shown in Fig. 5,
381   including the first eight members (those executed during 12:00 UTC 3 − 06:00 UTC 5
382   December), the middle eight members (run between 12:00 UTC 5 and 06:00 UTC 7
383   December), the last nine members (12:00 UTC 7−12:00 UTC 9 December), and the last
384   five members (12:00 UTC 8−12:00 UTC 9 December), respectively. In other words, the
385   last five members were those executed within 0-24 h (1 day) prior to the beginning of the
386   target period, and so on. In Fig. 5, it is clear that both the ensemble means from the last
387   five and the last nine members compare quite favorable to the observation, not only in the
388   accumulated amount but also in spatial distribution of rainfall. This indicates that the model
389   could produce QPFs at fairly good quality and rather consistently since the time as early as
390   roughly 48 h prior to the commencement of the rainfall event (also Fig. 3). These two sub-
391   ensemble groups within the short range gave much better quality in QPFs than the other
392   sub-groups executed before them at longer lead times, including the first eight, middle
393   eight, and all 25 members. In terms of skill scores, for example, the mean QPF by the last
394   five members have TS = 0.4, POD = 0.8, FB = 1.5, and FAR = 0.5 at 100 mm (per 24 h),
395   while the last nine members give similar scores of TS = 0.5, POD = 0.8, FB = 1.4, and
396   FAR = 0.5 (Figs. 6a-d), respectively. On the contrary, the mean QPFs from both the middle
397   eight and first eight members only yield zero scores in TS, POD, and FB with no skill in
398   FAR at 100 mm, obviously due to not enough rainfall in central Viet Nam in most of their
399   members. At 200 mm (per 24 h), similarly, the last five members (TS = 0.2, POD = 0.4,
400   FB = 1.4, and FAR = 0.7) and the last nine members (TS = 0.3, POD = 0.5, FB = 1.2, and
401   FAR = 0.6) again produce much better scores in QPFs, compared to no skill in all four
402   scores in QPFs from the middle eight, first eight, and all 25 members (Fig. 7a-d). In SSS,
403   the mean from the last nine members exhibits the highest score (0.64), the middle eight
404   members have the lowest score (0.04), and the mean from all 25 members is 0.43 (Fig. 6e).

405

406
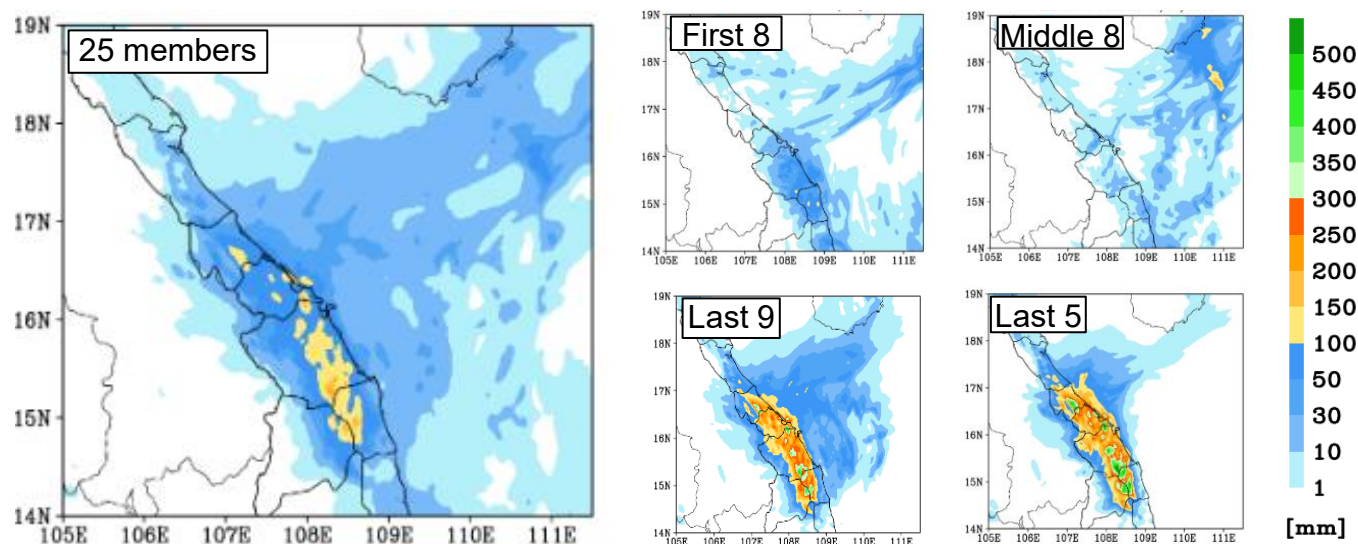
Figure 5. Ensemble mean rainfall (shaded, scale on the right) from all 25 time-lagged members, executed every 6 h from 12:00 UTC 3 December to 12:00 UTC 9 December, for the 24h period from 12:00 UTC 9 December to 12:00 UTC 10 December.
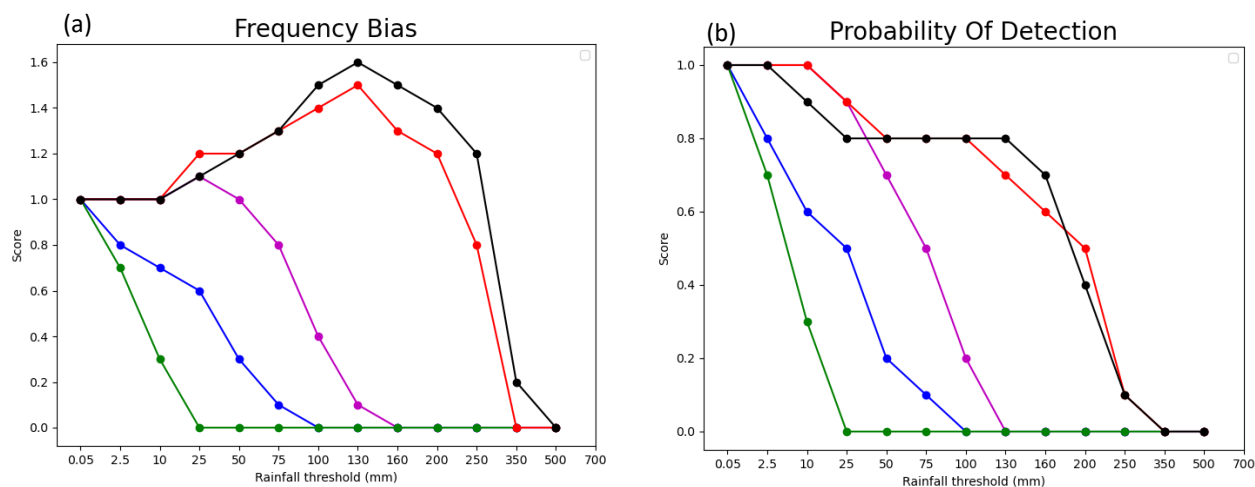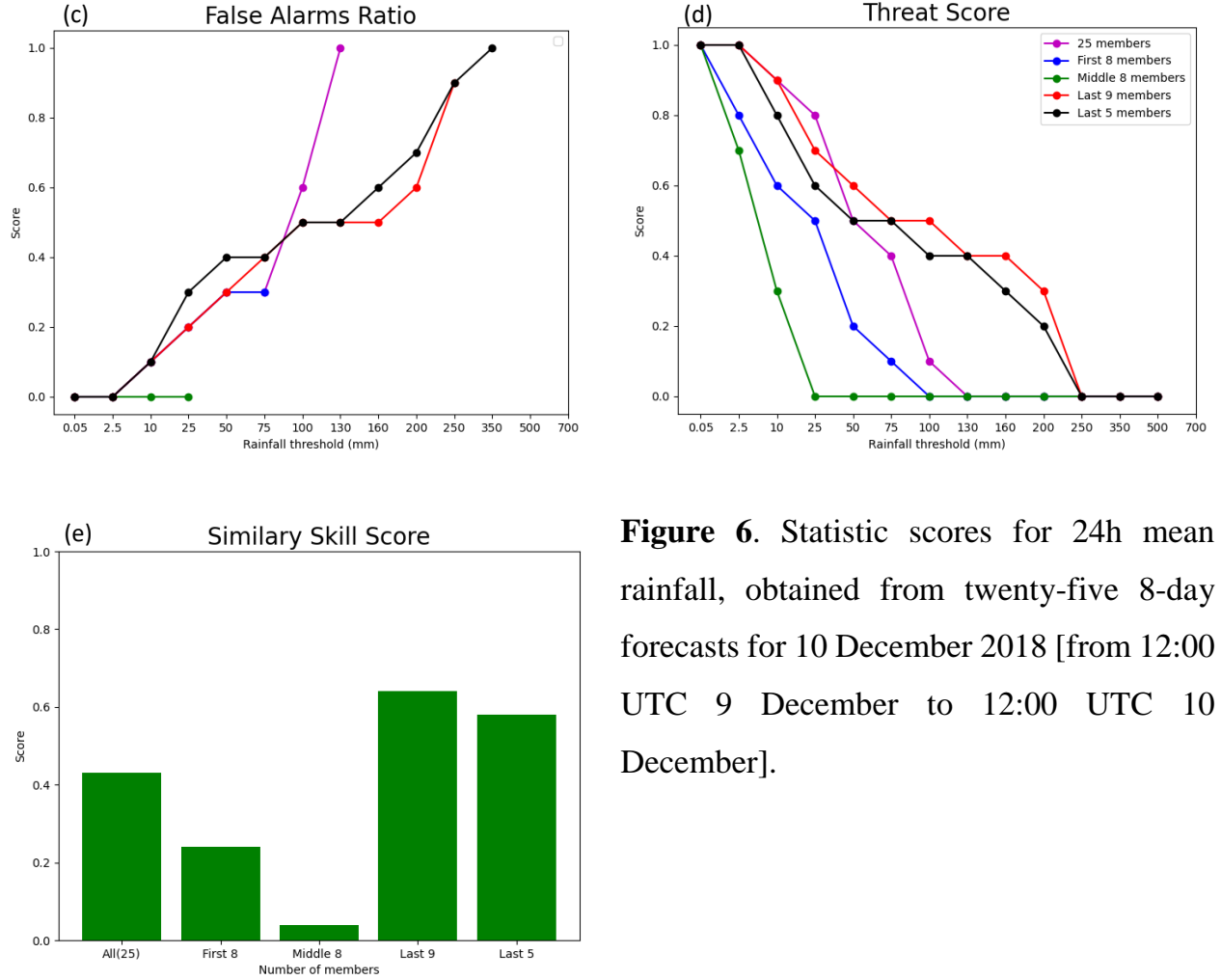
Figure 6. Statistic scores for 24h mean rainfall, obtained from twenty-five 8-day forecasts for 10 December 2018 [from 12:00 UTC 9 December to 12:00 UTC 10 December].

410

411   However, as indicated by the SD, the spreads in rainfall scenarios in both ensembles from

412   the last five and nine members are quite large (Fig. 7). Thus, while the lagged members

413   can produce a wide range of possible rainfall scenarios for the D18 event, which is the

414   main purpose of an ensemble as reviewed (Section 1), the members often cannot agree on

415   the precise locations of heavy rainfall. Given the small scale of local convection during the

416   event, this result is perhaps anticipated. On the other hand, the maxima in spread are >160

417   mm in Fig. 7 among the last nine members, and reasonable in magnitude compared to the

418   peak amounts of about 400 mm in the ensemble mean. In any case, Figs. 6 and 7 indicate

419   that the predictability of the D18 event changed considerably with time, and the 2.5-km

420 CReSS has a good skill in QPFs inside the short range (≤ 72 h). However, it is difficult to

421 predict the event successfully at longer lead times.

422

423

424
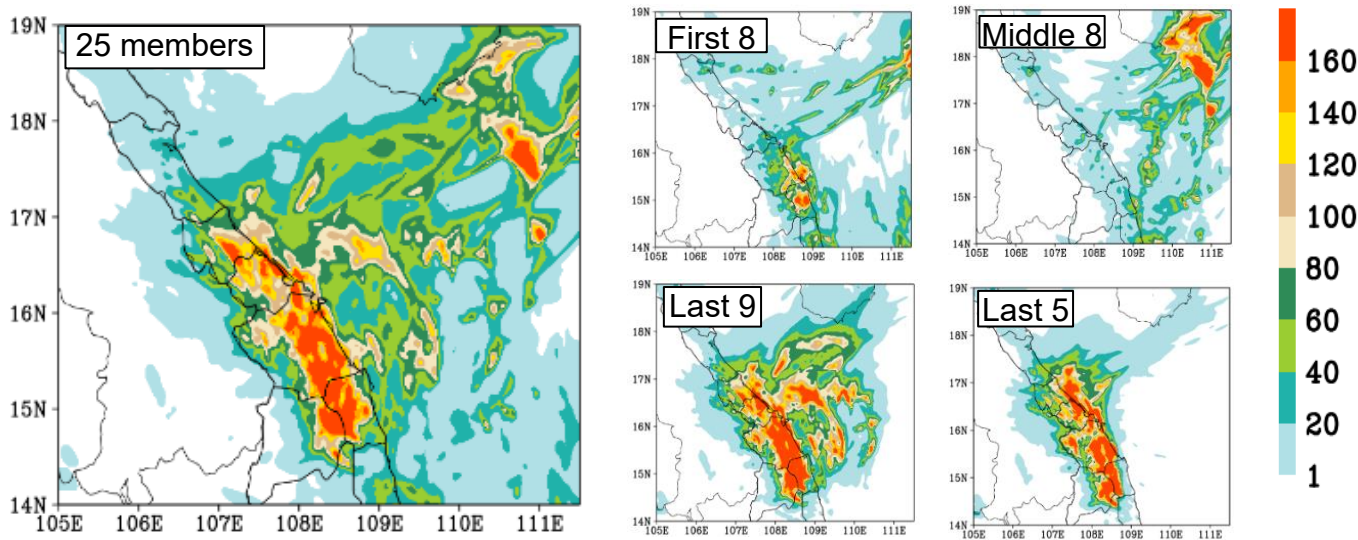
425 **Figure 7**. The spread (shaded, scale on the right) from all 25 time-lagged members,

426 executed every 6 h from 12:00 UTC 3 December to 12:00 UTC 9 December, for the 24h

427 period from 12:00 UTC 9 December to 12:00 UTC 10 December.

428

429 The probability information derived from the sub-ensemble groups at four different rainfall

430 thresholds from 100 to 450 mm is shown in Fig. 8, in which the increase in heavy-rainfall

431 probability in central Viet Nam and thus the predictability of the event with time is also

432 evident. From the first eight members executed at the longest range (≥ 102 h prior to rainfall

433 accumulation), there is only a 10-25% chance in parts of central Viet Nam to receive at

434 least 100 mm of rainfall (from 12:00 UTC 9 to 12:00 UTC 10 December). The probability

435 is even lower from the middle eight members (run between 54-96 h prior to target period),

436 as their SSS is the lowest among all sub-ensemble groups and only a couple of the runs

could reach 100 mm anywhere inland in central Viet Nam. As the lead time shortens to inside the short range, the probabilities to have ≥ 100 mm of rainfall increase dramatically, to roughly 70-80 % in the last nine members and further to over 80-90% in the last five members. Due to the contribution from later members, about 20-40% of all 25 members can reach 100 mm inland. Toward higher thresholds, the probabilities decrease in Fig. 8 as expected, so are the areal sizes actually reaching those thresholds (red contours). At the highest value of 450 mm, the ensembles in general show less than about 20% and 30% chances for its occurrence from the last five and last nine members, respectively, and the high probability areas are also slightly more inland than the observed one.
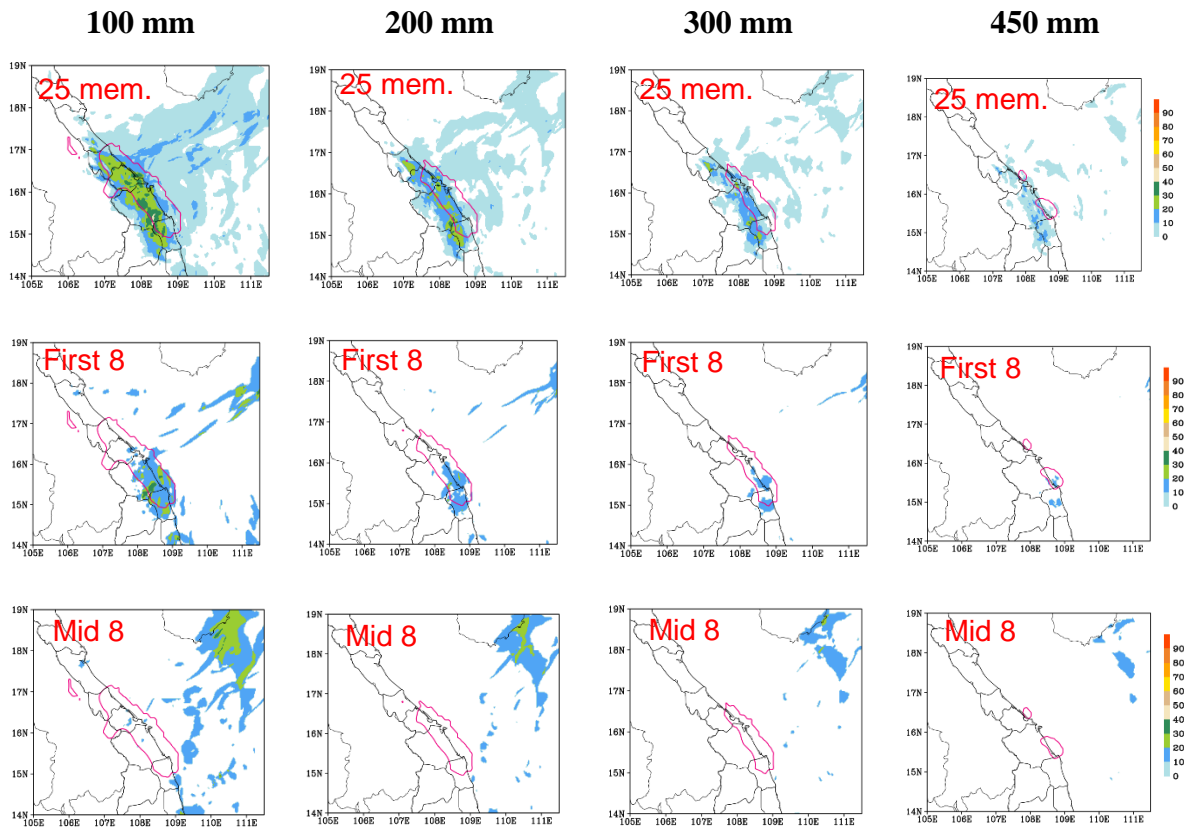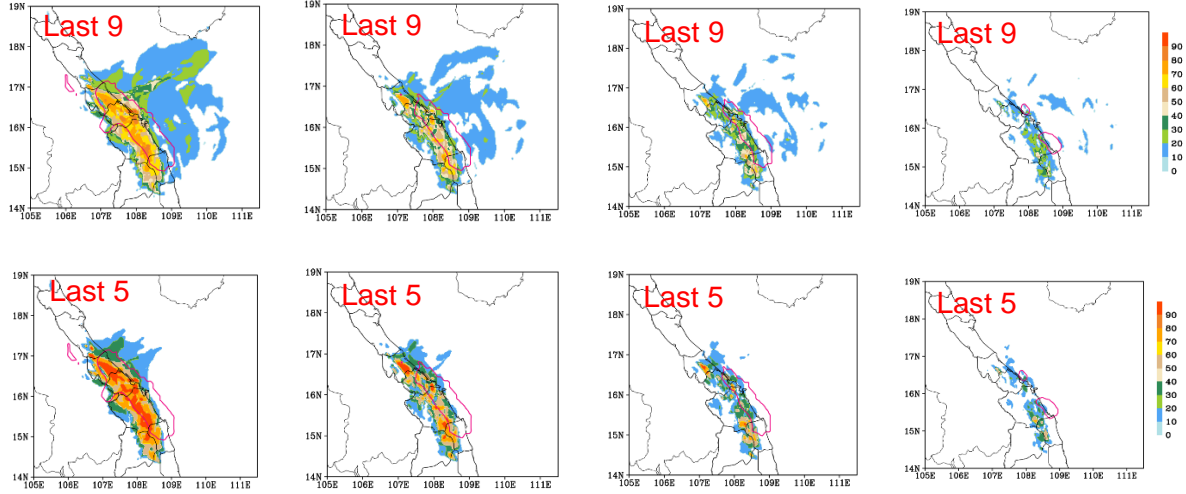
Figure 8. Probability distribution (%; shaded, scale on the right) from all 25 time-lagged members, executed every 6 h from 12:00 UTC 3 December to 12:00 UTC 9 December, reaching thresholds of 100, 200, 300, and 450 mm, for the 24h period from 12:00 UTC 9 December to 12:00 UTC 10 December. The observed areas at the same thresholds are depicted by the pink contours. For each picture, red labeled at the top-left corner show the number of members grouped to calculate the probability distribution.

3.2 Ensemble-based sensitivity analysis

The results in part 3.1 above reveal that the CReSS model with a horizontal resolution of 2.5 km had well QPF predicted the rainiest day of the event while other models can't capture it. Therefore, this part was made rely on this good performance.

Firstly, Figure 9 shown that the main reason for the significantly different forecast outcomes between five good members (those with initial times at 18:00 UTC on 4, 00:00, 06:00, and 12:00 UTC on 8, and 00:00 UTC on 9 December) and five bad ones (those ran at 18:00 UTC on 3, 18:00 UTC on 5, 06:00 and 18:00 UTC on 6, and 06:00 UTC on 7 December)(good minus bad members), is that there are significant differences in the input datasets. Specifically, the surface easterly winds were much stronger and the relative humidity much higher surrounding central Viet Nam and its upstream areas in the GFS forecast data valid at 12:00 UTC on 9 December (used as BCs in CReSS runs) in the good members than in the bad ones (Fig. 9a). These factors were identified as crucial for the

466   extreme rainfall in the D18 event in Part 1, and thus the good CReSS members produced

467   much more rainfall in central Viet Nam (Fig. 9b).

468
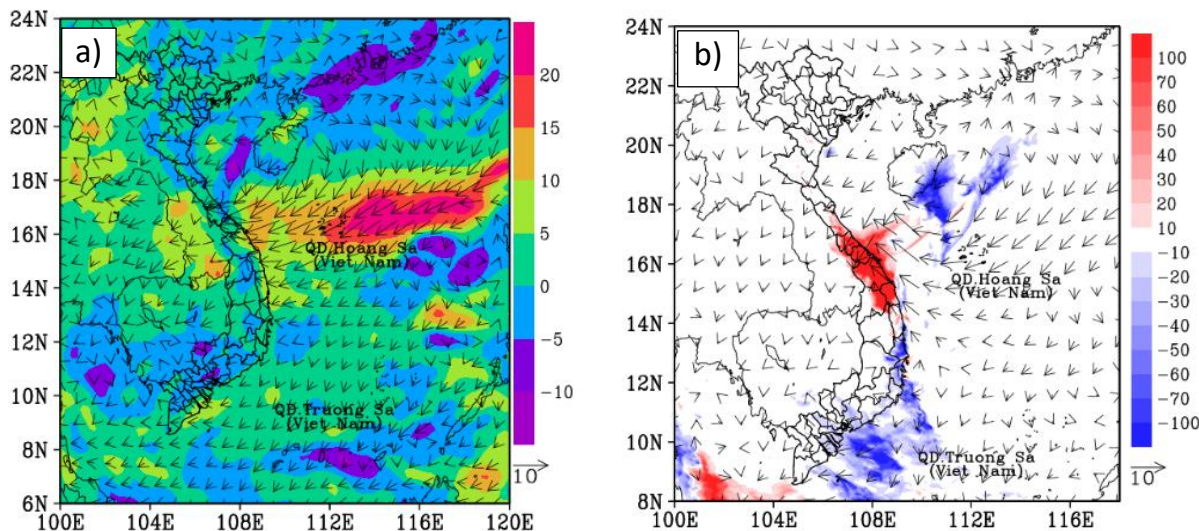
469   **Figure 9**. The difference in (a) input data (boundary conditions) and (b) CReSS output

470   between averaged 5 good members (members ran at 18:00 UTC 4, 00:00 UTC 8, 06:00

471   UTC 8, 12:00 UTC 8, 00:00 UTC 9) and 5 bad members (members ran at 18:00 UTC 3,

472   18:00 UTC 5, 06:00 UTC 6, 18:00 UTC 6, 06:00 UTC 7). For input data, relative humidity

473   (%, shaded) and surface wind (ms^{-1}, vector) at 12:00 UTC December 9 2018. For CReSS

474   output, 24-h accumulated rainfall (mm, shaded) and surface wind (ms^{-1}, vector).

475   Meanwhile, Figure 10 show the difference in the evolution of synoptic-scale patterns

476   (features), with a zoom in the study area. To be more specific, Figures 10a show the

477   difference (model output - NCEP FNL analysis data) in the horizontal wind and vertical

478   velocity between averaged 5 good members and the NCEP FNL analysis data at 925 hPa

479   and at 12 UTC 09 is small although each member was initialized at different lead time. It

480   implies that these members captured well the evolution of weather patterns of this event.

481   Additionally, the model vertical velocity is observed greater than NCEP FNL analysis data.

482   Therefore, these members produced the rainfall closer to observed rainfall even the study

483   area is a complex terrain. Contrarily, bad members poorly captured the evolution of

484   weather patterns (Fig. 10b). Consequently, these members can't produce rainfall close to

485   the observed rainfall data.

486   Furthermore, Figs. 10d indicates the difference in initial data of the member that initialized

487   at 18:00 UTC 04 is very small, especially over the study area. The evolution of weather

488   patterns every 24-hours based on this initial data is also observed small at first 3 days lead

489   time. The difference then developed larger. However, the difference is smaller at 12:00

490   UTC 09 (approximate 5 days lead time) (Figs. 10e,f,g). Compare to this, the bad member

491   initialized at 18:00 UTC 06 (2-days lead time shorter) have a larger difference in the

492   initialized state of atmosphere, even this difference is also small in comparison with NCEP

493   FNL analysis data (Fig. 10h). this difference then led to a larger difference in evolution of

494   weather patterns, as observed at Figs. 10 i, j, and k.

495

496

497
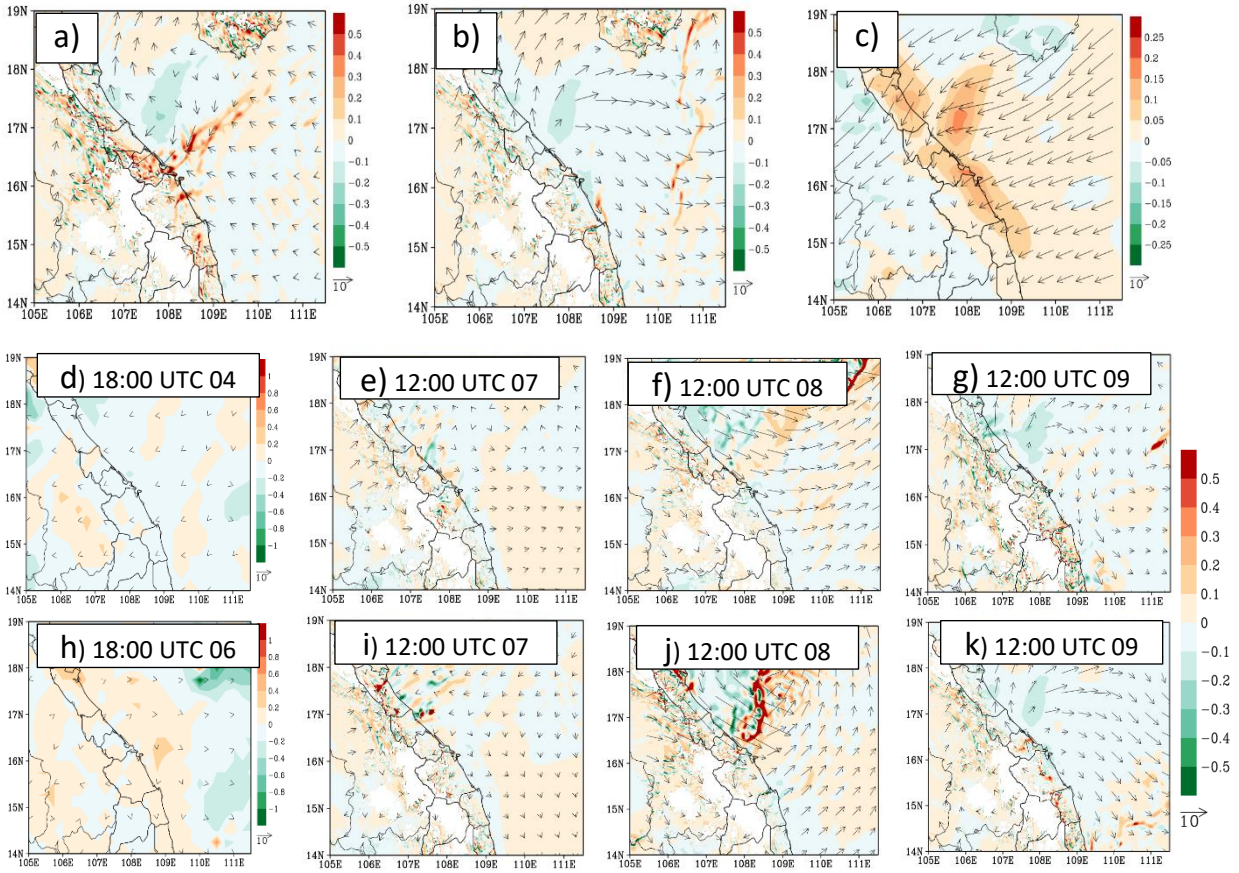
Figure 10. The difference in the horizontal wind (ms^{-1}, vector, reference length at the low-right corner of the panel), and vertical velocity (ms^{-1}, shaded, the reference color scale is on the right of panel) between (a) averaged 5 good members and (b) averaged 5 bad members and the NCEP FNL analysis data at 925 hPa and at 12 UTC 09. (c) The NCEP FNL analysis horizontal wind (ms^{-1}, vector, reference length at the low-right corner of the panel) and vertical velocity (ms^{-1}, shaded) at 925 mb and at 12 UTC 09. (d) The difference in the horizontal wind (ms^{-1}, vector, reference length at the low-right corner of the panel), and relative humidity (%, shaded, the reference color scale is on the right of panel) between the initial data of a good member at a longer lead time (at 1800 UTC 4 Dec) and the NCEP FNL analysis data at 925 hPa. (e), (f), and (g) present the difference in the evolution of weather features with time by this good member. (h) as in (d) but for a bad member (member was ran at 1800 UTC 6 Dec). (i), (j) and (k) as in (e), (f), and (g), respectively, but for mentioned bad member.

512   , (i), (j), and (k) by a bad member (member ran at 18 UTC 05).   Compared variables are

513   horizontal wind at 925 hPa (ms^{-1}, vector, reference length at the low-right corner of the

514   panel) and vertical velocity (ms^{-1}, shaded, the reference color scale is on the right of panel)

515   The NCEP FNL analysis horizontal wind (ms^{-1}, vector, reference length at the low-right

516   corner of the panel) and vertical velocity (ms^{-1}, shaded) at 925 mb and at 12 UTC 09.

517   These not only indicate that it is still possible to have good forecasts at a lead time of up to

518   5 days but also show the good performance of CReSS in predictability of the event at longer

519   lead time.

520   Additionally, these also reaffirm that a very small difference in the initialized data could

521   then lead to a very different in the outcome, especially as the forecast range increases. On

522   the other hand, the predicted rainfall is very sensitive with every small difference in the

523   initial data. Besides, as pointed out Part 1 that the low-level wind convergence led to

524   moisture convergence and these conditions resulted in the D18 event. And the southward

525   movement of the low-level wind convergence also dictated the movement of heavy

526   rainband during the event. Therefore, ESA was applied on relevant variables, including the

527   zonal and meridional components of wind, and water mixing ratio. The quantitative results

528   are shown in Figs. 11-13.

529   To be more specific, Figure 11 shows the sensitivity of mean 24-h total rainfall inside the

530   green box in central Viet Nam (R) to zonal (u) and meridional (v) wind components and

531   water vapor mixing ratio (q_v) at the surface, and the ensemble mean are also plotted. It is

532   clear that the sensitivity of rainfall to these variables is lower at longer forecast ranges and

533   becomes higher at shorter lead times. Specifically, from two days before (t_{-48}) to the

534   starting time of the accumulation period (t_0), the sensitivity of rainfall to u-wind over the

535   SCS and along the coast of central Viet Nam turned more negative, indicating heavier

536   rainfall associated with stronger easterly winds ($u < 0$) near the surface, especially in areas

537   immediately upstream at t_0 (Figs. 11a-d). The rainfall's sensitivity to v-wind leading to t_0,

538   on the other hand, exhibited a dipole structure, with negative values to the north-northwest

539 and positive values to the south-southeast across central Viet Nam and the upstream ocean.

540 This structure indicates a stronger confluence in northeasterly winds over the region in

541 rainier members, consistent with the results in Part 1. In Figs. 11e-h, the increase in *v*-wind

542 just south of central Viet Nam is particularly evident, from –10 mm (per SD, SD =2 ms^{-1})

543 at t_{-48} to over +70 mm (per SD – Standard deviation, SD=2-4 ms^{-1}) at t_0. Thus, the

544 precipitation amount in the D18 event in central Viet Nam is highly sensitive to the

545 northeasterly winds in short range forecasts.   Similarly, the rainfall was   also

546 highlysensitive to the water vapor amount as shown in Figs. 11i-l.
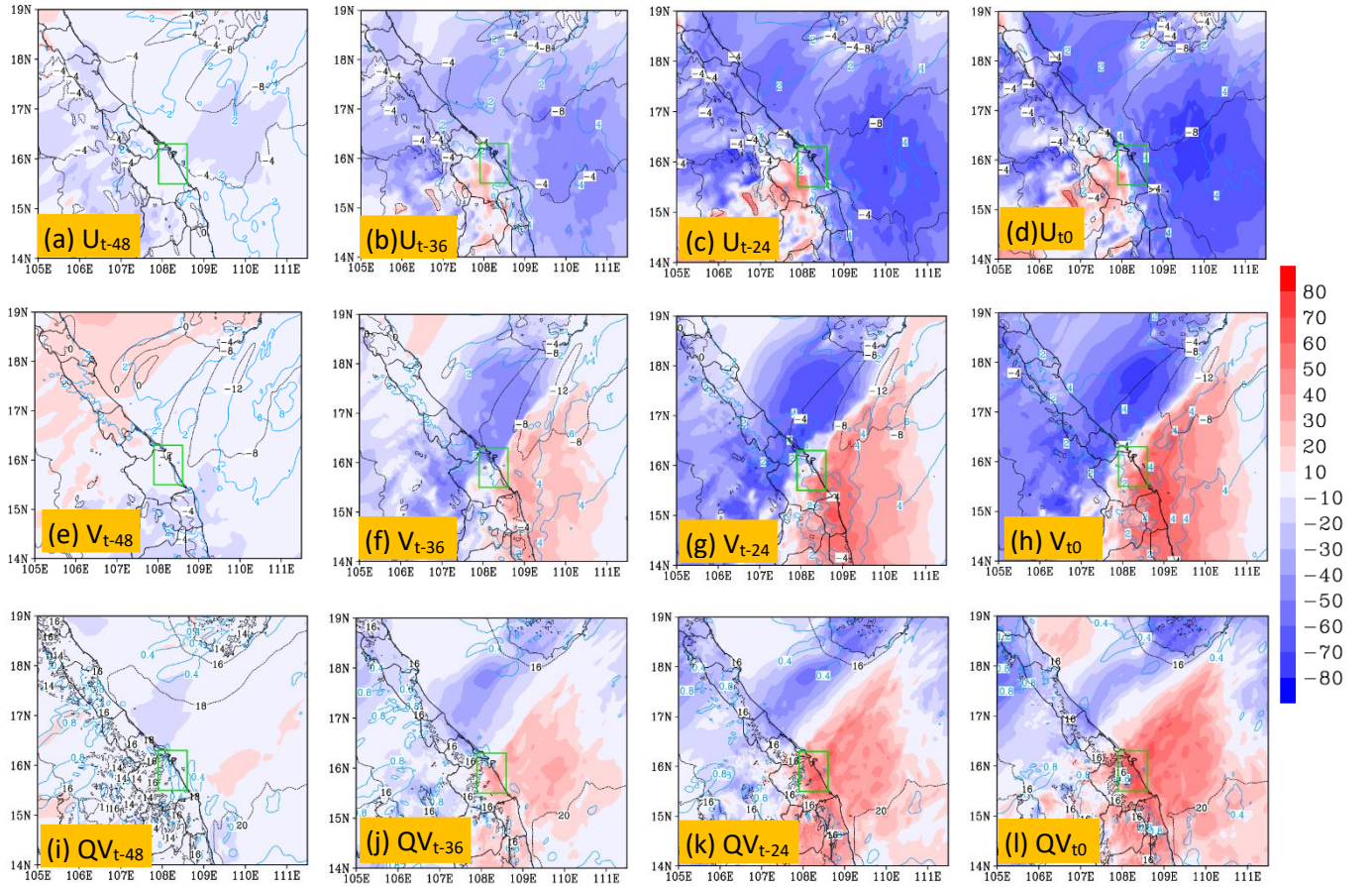
547 **Figure 11**. The sensitivity (mm, per SD, color, scale on the right) of areal-mean 24h

548 accumulated rainfall in central Viet Nam starting from t_0 (i.e., R, averaging area depicted

549 in green box) to surface wind components (ms^{-1}, shaded) and the ensemble mean (contours,

550 every 4 ms^{-1}) and to surface water vapor mixing ratio (r, g kg^{-1}) and its ensemble mean

551 (contours, every 0.06 g kg^{-1}) at different times at 24h intervals from (a) t$_{-48}$ to (f) t$_0$. The

552 time of t$_0$ is 12:00 UTC 9 December 2018. In which, (a), (b), (c), (d) for the zonal wind

553 component. (e), (f), (g), (h) for the meridional wind component, and (i), (j), (k), (l) for

554 surface water vapor mixing ratio. The standard deviation is exhibited by the medium blue

555 contours.

556 Slightly higher at 1476 m (near 850 hPa), where easterly flow prevailed during the D18

557 event (see Fig. 3b in Part 1), the sensitivity of rainfall to winds exhibits similar spatial

558 patterns (Figs. 12a-h) to those at the surface (Figs. 11a-h), with stronger easterly winds and

559 larger confluence in association with heavier rainfall. Similarly, the rainfall still shows

560 high sensitive to mixing ratio in central Viet Nam at this level (Figs. 12i-l), especially at

561 shorter lead times,. Presumably, this positive correlation is due to upward transport of

562 moisture, as the ascending motion in convective clouds could become larger at this level.

563

564

565

566

567

568

569

570

571
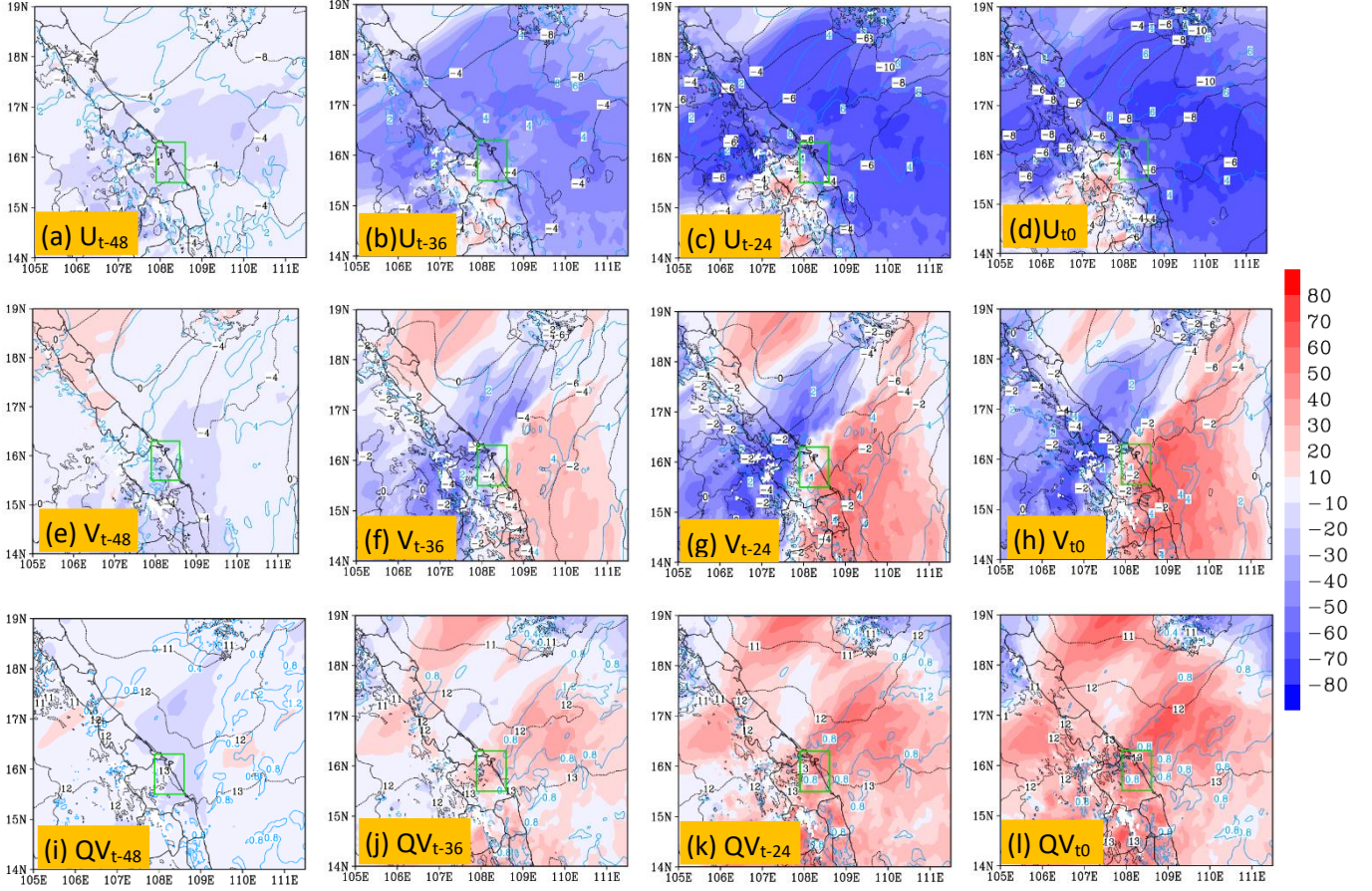
Figure 12. The sensitivity (mm, per SD, color, scale on the right) of 24h accumulated rainfall in central Viet Nam starting from t_0 (i.e., R, averaging area depicted in green box) to the wind components (ms^{-1}, shaded) and the ensemble mean (contours, every 2 ms^{-1}) and to water vapor mixing ratio (r, g kg^{-1}) and its ensemble mean (contours, every 0.4 g kg^{-1}) at attitude of 1476 m and at different times at 24h intervals from (a) t_{-48} to (f) t_0. The time of t_0 is 12:00 UTC 9 December 2018. In which, (a), (b), (c), (d) for the zonal wind component. (e), (f), (g), (h) for the meridional wind component, and (i), (j), (k), (l) for water vapor mixing ratio. The standard deviation is exhibited by the medium blue contours.

┐┐

At the upper level of 5424 m (near 500 hPa), it is seen that from t_{-48} to t_0, dipole structures developed in the sensitivity patterns to both u and v winds (Figs. 13a-h). To u winds, positive sensitivity up to about +70 mm (per SD, SD=2-4 ms^{-1} depends on t_x) existed to the

584   south and negative sensitivity up to −70 mm (per SD, SD=2-4 ms^{-1} depends on t_x) to the

585   north of central Viet Nam. Meanwhile, positive sensitivity to v-wind appeared to the north

586   and east with negative sensitivity to the south and west of the rainfall area. While the

587   prevailing winds at 500 hPa were southeasterly over southern Viet Nam and southwesterly

588   over northern Viet Nam during D18 (thus with anticyclonic curvature, see Fig. 3c in Part

589   1), the above sensitivity patterns, apparent at t_{-24} already, corresponded to stronger

590   diffluence/divergence and a weaker anticyclone aloft to favor more rainfall. To q_v, positive

591   sensitivity signals up to +70 mm (per SD, SD=1.2 g kg^{-1}) also appeared over the rainfall

592   area at t_{-24} and t_0 (Figs. 13i-l), and the reason is similar to those near 850 hPa in Fig. 11.
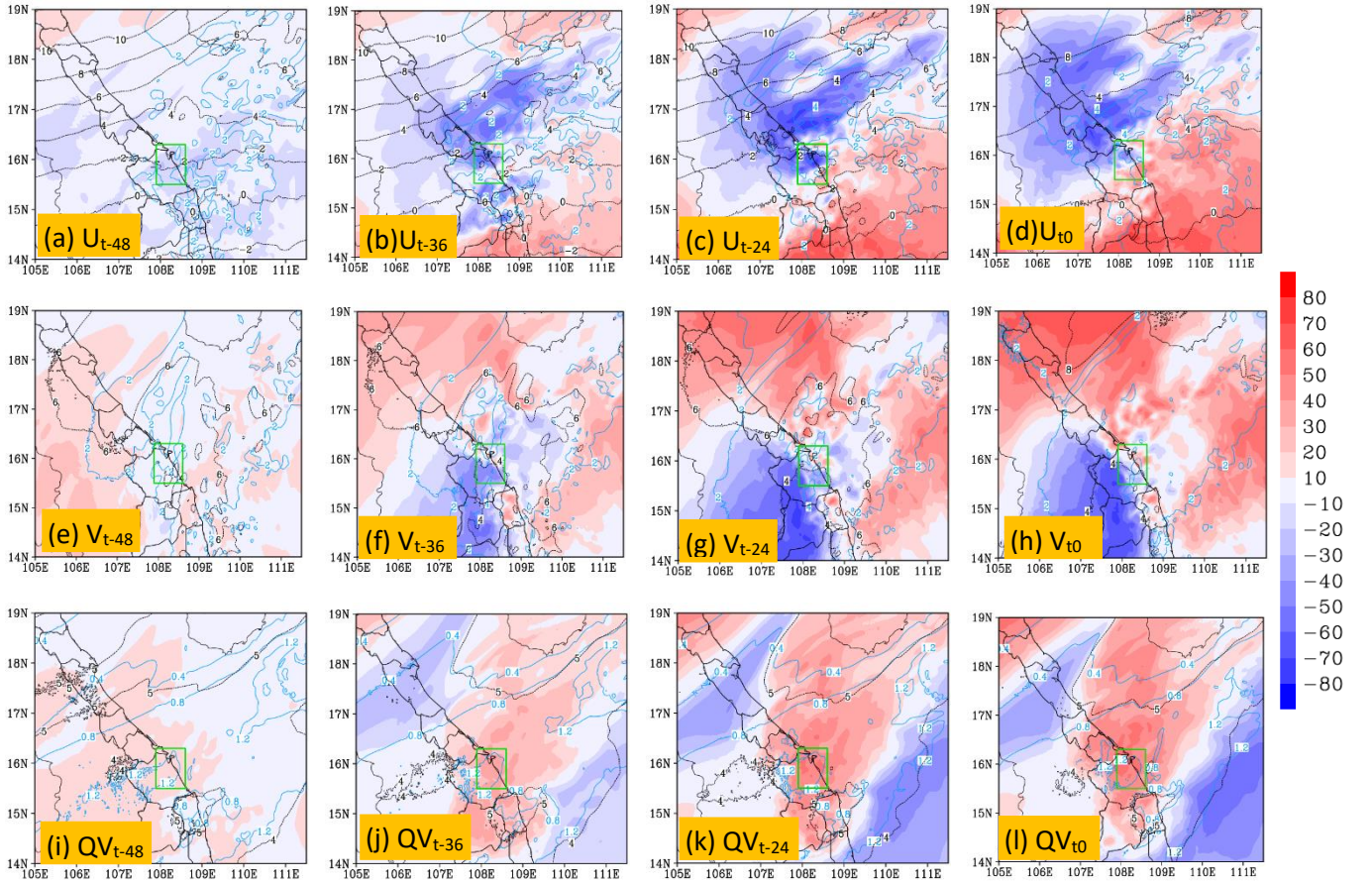
593   **Figure 13**. The sensitivity (mm, per SD, color, scale on the right) of 24h accumulated

594   rainfall in central Viet Nam starting from t_0 (i.e., R, averaging area depicted in green box)

595   to the wind components (ms^{-1}, shaded) and the ensemble mean (contours, every 2 ms^{-1})

596   and to water vapor mixing ratio (r, g kg^{-1}) and its ensemble mean (contours, every 0.4 g kg^{-1})

597   ^{1}) at attitude of 5424 m and at different times at 24h intervals from (a) t$_{-48}$ to (f) t$_0$. The

598   time of t$_0$ is 12:00 UTC 9 December 2018. In which, (a), (b), (c), (d) for the zonal wind

599   component. (e), (f), (g), (h) for the meridional wind component, and (i), (j), (k), (l) for

600   water vapor mixing ratio. The standard deviation is exhibited by the medium blue contours.

601   These ensemble-based sensitivity analyses indicated clearly that the synoptic pattern that

602   caused the D18 event already developed at times more than 24h earlier.

4 Conclusion

604   As high resolution is required in numerical models to predict heavy rainfall more

605   successfully, the present work utilizes a time-lagged high-resolution ensemble forecast

606   system and evaluates how well the D18 event (during 9-12 December 2018) in central Viet

607   Nam can be predicted in advance before its occurrence. Using the CReSS model with a

608   grid size of 2.5 km (912 × 900 in dimension with 60 vertical levels), ensemble forecasts

609   were produced with a total of 29 time-lagged runs at 6-h intervals, each out to a forecast

610   range of 192 h (eight days). Our evaluation results in predictability indicate that the 2.5-

611   km system predicted the rainfall fields on 10 December during the event fairly well,

612   including both the amount and spatial distribution, within the short range at lead times of

613   day 1, 2, and 3. More specifically, the SSS of QPFs at these three ranges are about 0.4, 0.6,

614   and 0.7, respectively, with fairly consistent results among successive runs that indicate a

615   reasonable predictability, despite some spread and disagreement on the precise locations

616   of heavy rainfall. The above good results are due to the model's capability to better predict

617   the conditions in the lower troposphere such as the wind fields.

618   At lead times longer than three days, however, the predictability of the event is lowered

619   due to a higher level of forecast uncertainty, and the quality of QPFs drops with significant

620   under-prediction. Nevertheless, good QPFs are still possible occasionally. At lead time

621   beyond six days, it is challenging to achieve a good QPF at thresholds greater than 100 mm

622   even with a high-resolution model. This is presumably linked to the rapid evolution of

atmospheric conditions surrounding Viet Nam in a tropical environment. In the present study, a CRM is applied to forecast extreme rainfall in central Viet Nam for the first time. Although still with certain limitations, our results do indicate hope to predict such events successfully beforehand, at least within the short range. Therefore, based on the present work, more studies on the predictability of extreme rainfall in Viet Nam are recommended in the near future.

The present study also performed an ensemble sensitivity analysis to identify the important factors that influenced the 24-h rainfall amount in central Viet Nam in the D18 event. The result shows that the rainfall is most sensitive to the wind conditions in the lower troposphere leading to the event, with more rain associated with stronger northeasterly to easterly winds and their confluence. Similarly, the rainfall also shows strong sensitivity to the moisture amount, not only at the surface but also further aloft at the upper levels. Besides, ESA also indicated that the synoptic pattern that caused the D18 event already developed at timing earlier in the past. Furthermore, in the ESA, the finer-scale features (convection) are also seen to link to synoptic conditions in their background, implying that it is meaningful to apply ESA to control the perturbations in initial fields.

Acknowledgements: This study was supported by the project "*Research on the application of the Cloud-resolving model integrated with the regional numerical model to a 6-hour accumulated quantitative precipitation forecast with 24-48 hours lead time for Mid-Central Viet Nam*", which is funded by the Ministry of Natural Resources and Environment (MONRE) under grant no. TNMT.2023.06.07, and also by the National Science and Technology Council (NSTC) of Taiwan under grants MOST 111-2111-M-003-005 and MOST 111-2625-M-003-001.

Code and data availability. The CReSS model used in this study and its user's guide are available at the model website at http://www.rain.hyarc.nagoya-

u.ac.jp/~tsuboki/cress_html/src_cress/CReSS2223_users_guide_eng.pdf (last access: 6 July 2023; Tsuboki and Sakakibara, 2007). The TIGGE data and its information are available at https://confluence.ecmwf.int/display/TIGGE/TIGGE+archive. The NCEP GFS dataset and its description are available at https://rda.ucar.edu/datasets/ds084.1/. The NCEP FNL operational global gridded analysis data and its information is available at https://rda.ucar.edu/datasets/d083003/#.

Author contributions. **Duc Van Nguyen** prepared datasets, executed the model experiments, performed the analysis, and prepared the first draft of the manuscript. **Chung-Chieh Wang** also prepared the first draft and provided the funding, guidance and suggestions during the study, and they participated in the revision of the manuscript. **Kien Ba Truong** provided the funding and participated revising of the manuscript. **Thang Van Vu**, **Pham Thi Thanh Nga**, and **Pi-Yu Chuang** also participated in the revision of the manuscript.

Competing interests. The authors declare that they have no conflict of interest.

References

Ancell, and Hakim, G. J.: Comparing adjoint- and ensemble sensitivity analysis with applications to observation targeting. Mon. Wea. Rev., 135, 4117–4134, doi:10.1175/2007MWR1904.1, 2007.

Cotton, W. R., Tripoli, G. J., Rauber, R. M., and Mulvihill, E. A.: Numerical simulation of the effects of varying ice crystal nucleation rates and aggregation processes on orographic snowfall. J. Appl. Meteorol. Clim., 25, 1658–1680, 1986.

Coleman,A. A., and Ancell, B. C.:Toward the improvement of high-impact probabilistic forecasts with a sensitivity-based convective-scale ensemble subsetting technique. Mon. Wea. Rev., 148, 4995–5014, https://doi.org/10.1175/MWRD-20-0043.1, 2020.

675 Deardorff, J. W.: Stratocumulus-capped mixed layers derived from a three-dimensional
676   model. Bound.-Lay. Meteorol., 18, 495–527, 1980.

677 Hu, C.-C., and Wu, C.-C.: Ensemble sensitivity analysis of tropical cyclone
678   intensification rate during the development stage. J. Atmos. Sci., 77, 3387–
679   3405, https://doi.org/10.1175/JAS-D-19-0196.1, 2020.

680 Hoa, V. V.: Comparative study skills rain forecast the middle part and central highland of
681   several global models (In Viet Namese). Viet Nam journal of Hydrometeorology. V.
682   667 No. 07 (2016), 2016.

683 Hohenegger, C., and Schär, C.: Predictability and error growth dynamics in
684   cloud-resolving models. J. Atmos. Sci., 64, 4467–4478,
685   https://doi.org/10.1175/2007JAS2143.1, 2007.

686 Ikawa, M. and Saito, K.: Description of a non-hydrostatic model developed at the Forecast
687   Research Department of the MRI, MRI Technical report 28, Japan Meteorological
688   Agency, Tsukuba, Japan, ISSN: 0386-4049, 1991.

689 Kerr, C. A., Stensrud, D. J. and Wang, X.: Diagnosing convective dependencies on near-
690   storm environments using ensemble sensitivity analyses. Mon. Wea. Rev., 147, 495–
691   517, https://doi.org/10.1175/MWRD-18-0140.1, 2019.

692 Kondo, J.: Heat balance of the China Sea during the air mass transformation experiment.
693   J. Meteorol. Soc. Jpn., 54, 382–398, https://doi.org/10.2151/jmsj1965.54.6_382, 1976.

694 Leith, C. E.: Theoretical skill of Monte Carlo forecasts. Mon. Wea. Rev., 102, 409–
695   418, 1974.

696 Lin, Y.-L., Farley, R. D., and Orville, H. D.: Bulk parameterization of the snow field in a
697   cloud model. J. Appl. Meteorol. Clim., 22, 1065–1092, 1983.

698 Louis, J. F., Tiedtke, M., and Geleyn, J. F.: A short history of the operational PBL
699   parameterization at ECMWF, in: Proceedings of Workshop on Planetary Boundary

Layer Parameterization, 25– 27 November 1981, Shinfield Park, Reading, UK, 59–79, 1982.

Lorenz, E.N.: The predictability of a flow which possesses many scales of motion. Tellus, 21, 289–307. https://doi.org/10.3402/tellusa.v21i3.10086, 1969.

Murphy, J. M.: The impact of ensemble forecasts on predictability. Quart. J. Roy. Meteor. Soc., 114, 463–493, 1988.

Murakami, M.: Numerical modeling of dynamical and microphysical evolution of an isolated convective cloud – the 19 July 1981 CCOPE cloud. J. Meteorol. Soc. Jpn., 68, 107–128, 1990.

Murakami, M., Clark, T. L., and Hall, W. D.: Numerical simulations of convective snow clouds over the Sea of Japan: Two dimensional simulation of mixed layer development and convective snow cloud formation. J. Meteorol. Soc. Jpn. 72, 43–62, 1994.

Nhu, D. H., Anh, N. X., Phong, N. B., Quang, N. D., and Hiep, V. N.: The role of orographic effects on occurrence of the heavy rainfall event over central Viet Nam in November 1999. Journal of Marine Science and Technology. V. 17, No. 4B(2017), 31-36, 2017.

Segami, A., Kurihara, K., Nakamura, H., Ueno, M., Takano, I., and Tatsumi, Y.: Operational mesoscale weather prediction with Japan Spectral Model. J. Meteorol. Soc. Jpn., 67, 907–924, https://doi.org/10.2151/jmsj1965.67.5_907, 1989.

Surcel, M., Zawadzki, I., and Yau, M. K.: On the filtering properties of ensemble averaging for storm-scale precipitation forecasts. Mon. Wea. Rev., 142, 1093–1105, doi:10.1175/ MWR-D-13-00134.1, 2014.

Son, B. M. and Tan, P. V.: Experiments of heavy rainfall prediction over South of Central Viet Nam using MM5 (In VietNamese). Viet Nam Journal of Hydrometeorology., 4(580), 9−18, 2009.

Toan, T. N., Thanh, C., Phuong, P. T., and Anh, T. V.: Assessing the predictability of WRF model for heavy rain by cold air associated with the easterly wind at high-level patterns over mid-central Viet Nam (In VietNamese). VNU Journal of Science: Earth and Environmental Sciences. v. 34, n. 1S, dec. 2018. ISSN 2588-1094. https://js.vnu.edu.vn/EES/article/view/4328, 2018.

Torn, R.D., Hakim, G.J.: Initial condition sensitivity of western Pacific extratropical transitions determined using ensemble-based sensitivity analysis. Mon. Weather Rev. 137, 3388–3406. https://doi.org/10.1175/2009MWR2879.1, 2009.

Tsuboki, K. and Sakakibara, A.: Numerical Prediction of HighImpact Weather Systems: The Textbook for the Seventeenth IHP Training Course in 2007, Hydrospheric Atmospheric Research Center, Nagoya University, Nagoya, Japan, and UNESCO, Paris, France, 273 pp., http://www.rain.hyarc.nagoya-u.ac.jp/~tsuboki/ cress_html/src_cress/CReSS2223_users_guide_eng.pdf (last access: 1 May 2019), 2007.

Tuoi Tre news: https://tuoitre.vn/mien-trung-tiep-tuc-mua-lon-14-nguoi-chet-va-mat-tich-20181212201907413.htm (last ac-cess: 5 June 2024), 2018

Wang, C.-C.*, Kuo, H.-C., Yeh, T.-C., Chung, C.-H., Chen, Y.-H., Huang, S.-Y., Wang, Y.-W., and Liu, C.-H.: High-resolution quantitative precipitation forecasts and simulations by the Cloud-Resolving Storm Simulator (CReSS) for Typhoon Morakot (2009). J.Hydrol., 506, 26-41, http://dx.doi.org/10.1016/j.jhydrol.2013.02.018, 2013.

Wang. C.-C.*, Lin, B.-X., Chen, C.-T., and Lo, S.-H.: Quantifying the effects of long-term climate change on tropical cyclone rainfall using cloud-resolving models: Examples of two landfall typhoons in Taiwan. J. Climate, 2015.

Wang, C.-C.: On the calculation and correction of equitable threat score for model quantitative precipitation forecasts for small verification areas: The example of Taiwan. Wea. Forecasting, 29, 788–798, doi:10.1175/WAF-D-13-00087.1, 2014.

751 Wang, C.-C., Huang, S.-Y., Chen, S.-H., Chang, C.-S., and Tsuboki, K.: Cloud resolving

752   typhoon rainfall ensemble forecasts for Taiwan with large domain and

753   extended range through time-lagged approach. Wea. Forecasting, 31,151–172,

754   doi:10.1175/WAF-D-15-0045.1, 2016.

755 Wang, C.-C., Li, M.-S., Chang, C.-S., Chuang, P.-Y., Chen, S.-H., and Tsuboki, K.:

756   Ensemble-based sensitivity analysis and predictability of an extreme rainfall event

757   over northern Taiwan in the Mei-yu season: The 2 June 2017 case. Atmos. Res., 259,

758   105684, https://doi.org/10.1016/j.atmosres.2021.105684, 2021.

759 Wang, C.-C., Tsai, C.-H., Jou, B. J.-D., and David, S. J.: Time-Lagged Ensemble

760   Quantitative Precipitation Forecasts for Three Landfalling Typhoons in the Philippines

761   Using the CReSS Model, Part I: Description and Verification against Rain-Gauge

762   Observations. Atmosphere, 13, 1193, https://doi.org/10.3390/atmos13081193, 2022.

763 Wang, C.-C., and Nguyen, D. V.: Investigation of an extreme rainfall event during 8–12

764   December 2018 over central Viet Nam – Part 1: Analysis and cloud-resolving

765   simulation. Nat. Hazards Earth Syst. Sci., 23, 771–788, https://doi.org/10.5194/nhess-

766   23-771-2023, 2023.

767 Wang, C.-C., Chen, S.-H., Chen, Y.-H., Kuo, H.-C., Ruppert, Jr., J. H., and Tsuboki, K.:

768   Cloud-resolving time-lagged rainfall ensemble forecasts for typhoons in Taiwan:

769   Examples of Saola (2012), Soulik (2013), and Soudelor (2015). Wea. Clim. Extremes,

770   40, 100555, https://doi.org/10.1016/j.wace.2023.100555, 2023.

771 Wilks, D. S.: Statistical Methods in the Atmospheric Sciences. Academic Press, 648 pp.,

772   ISBN 13: 978-0-12-751966-1, 10: 0-12- 751966-1, 2006.

773